[American Journal of Science, Vol. 305, May, 2005, P. 407–448]

CHRONOLOGICAL CONSTRAINTS ON THE PRE-OROGENIC HISTORY, BURIAL AND EXHUMATION OF DEEP-SEATED ROCKS ALONG THE EASTERN MARGIN OF THE VARISCAN OROGEN, BOHEMIAN MASSIF, CZECH REPUBLIC

KAREL SCHULMANN*, ALFRED KRÖNER**, ERNST HEGNER***, IMMO WENDT***, JIŘÍ KONOPÁSEK****·******, ONDREJ LEXA*·****, and PAVLA ŠTÍPSKÁ*·****

ABSTRACT. Key lithological units of the high-grade eastern margin of the Bohemian Massif were dated using the U-Pb and Pb-Pb methods on zircons in order to establish a chronological framework for the geodynamic evolution of the Variscan orogenic root. The protolith ages for metagranitoids, orthogneisses and granulites of thickened lower and middle crust reveal the existence of magmatic activity that occurred over a 100 million year time interval from Cambro-Ordovician to early Devonian times, probably related to discontinuous intracontinental rifting of Neoproterozoic crust. Our geochronological data suggest that the eastern part of the orogenic root represents thermally softened and rifted Neoproterozoic crust, preserved farther to the east as the Brunia microcontinent. Zircon ages for felsic granulites, high-grade gneisses of the lower crust and of a syn-convergence granodioritic intrusion in the upper crust indicate that thickening and exhumation of the crust occurred during a narrow time interval between 370 and 340 Ma. Exhumation of the lower crust to mid-crustal levels was a localized process that occurred at ~340 Ma and was associated with crustal-scale folding in the internal part of the root as well as orogenic channel flow along the eastern collisional margin. Both types of exhumation mechanisms were driven by deep-level wedging (indentation) of the easterly Brunia continent, followed by deposition of heavy minerals and pebbles derived from high-pressure rocks in the adjacent foreland basin. Final orogenic development was characterized by NE-SW dextral transpressive shearing parallel to the Brunia margin as well as dextral transtension associated with activity along the Elbe lithospheric fault. These processes affected the marginal parts of the orogenic root and were accompanied by 330 to 325 Ma old syntectonic granitoid intrusions along reactivated lithotectonic boundaries. Rotation of the assembled orogenic belt, accompanied by lithospheric faulting driven by westerly subduction roll-back, may be the most plausible model to explain late deformation of the orogenic root.

INTRODUCTION

Thickened orogenic root systems form during prolonged convergence of lithospheric plates (Dewey and Bird, 1970). Crustal thickening during collision is generally associated with intense ductile deformation and high-grade metamorphism with peak pressure conditions corresponding to double average crustal thickness, and temperatures permitting for extensive melting to occur in mica- and amphibole-rich rocks (Thompson, 1999). An important consequence of melting of rocks buried to the bottom of an orogenic root is the obliteration of the pre-collisional history of most rock assemblages and resetting of many isotopic systems. The exhumation of such deeply buried rocks late in the collisional history may also involve further decompression

*Université Louis Pasteur, Centre de Geochimie de la Surface, UMR-CNRS 7517, 1 rue Blessig, 67084 Strasbourg cedex, France; schulman@illite.u-strasbg.fr
**Institut für Geowissenschaften, Universität Mainz, 55099 Mainz, Germany
***Department für Geo- und Umweltwissenschaften, Universität München, Theresienstrasse 41, 80333 München, Germany
****Institute of Petrology and Structural Geology, IPSG, Charles University, Albertov 6, CS 12843 Prague, Czech Republic
*****Czech Geological Survey, Klarov 3, Prague, 11821, Czech Republic

melting. Another consequence of exhumation processes within orogenic root systems is juxtaposition of crustal units showing distinctly different peak pressure metamorphic records (Štípská and others, 2004). The intrusion of syntectonic granitoids frequently follows important structural boundaries of exhumed units and, because of rapid cooling, these intrusive rocks best record the timing of melting processes in the remaining root.

Lithotectonic units with specific P-T histories may be assigned to lower, middle, and upper crustal segments. However, this interpretation neglects the depositional and early orogenic evolution of supracrustal and pre-orogenic intrusive assemblages. Therefore, rocks forming the orogenic root of a collisional system are often not placed and interpreted in terms of their pre-collisional paleogeographic geodynamic setting and position in the crust.

The U-Pb and Pb-Pb isotopic systems in zircon are very resistant to even high-grade metamorphism and so may be used to extract information on older events such as primary magmatism and initial metamorphism, despite multiple phases of high-grade metamorphism (Mezger and Krogstad, 1997; Möller and others, 2002). This behavior offers the opportunity to obtain information on the timing of early magmatic events prior to formation of the orogenic root and on late melting events associated with maximum burial and exhumation of the host rocks. Therefore, deciphering the P-T evolution of an orogenic root, combined with precise dating of individual high-T events, provides a basis for understanding the mechanisms of formation and exhumation of orogenic root systems through time.

The Variscan orogen in Europe represents such a hot orogenic root system (Dewey and Burke, 1973) which allows observation of the finite metamorphic and structural patterns at considerable detail that cannot be studied in active modern orogens. The Variscan orogeny occurred during Devonian to Carboniferous convergence of peri-Gondwanan crustal segments and the northern European plate, also known as Baltica (Ziegler, 1986; Tait and others, 1996). Prior to this convergence all Neoproterozoic units forming the Bohemian Massif (the Saxothuringian, the Teplá Barrandian and Moldanubian domains; Franke, 1989) were affected by large-scale Cambro-Ordovician rifting processes which are commonly interpreted as a result of fragmentation of the northern Gondwana margin and drift of lithospheric terranes to the north (Kröner and others, 2000b; Štípská and others, 2001; Friedl and others, 2004; this work). During the early Devonian a major switch in plate movement occurred, resulting in the development of the SE-dipping Saxothuringian subduction zone (in present-day coordinates) (Franke, 2000). This paleo-subduction zone is characterized by the development of high-pressure, low-temperature metamorphism during the Devonian and obduction of eclogites on top of the Saxuthuringian plate (Franke, 2000). The Saxothuringian oceanic and continental crust were subducted underneath an upper continental plate that is today represented by the Teplá-Barrandian and Moldanubian domains (fig. 1), and this subduction created a large-scale magmatic arc in the area of Central Bohemian Pluton (Žák and others, 2005). Carboniferous collision of the Saxothuringian plate with the hanging-wall Teplá-Barrandian and Moldanubian domains involved major crustal thickening and development of an internal orogenic zone represented by a thickened orogenic root that is exposed today between the Saxothuringian domain in the northwest and the late Neoproterozoic Brunia terrane in the southeast (Dudek, 1980).

The lack of precise protolith ages for rocks constituting the principal units of the Moldanubian domain has so far prevented an in-depth understanding of its development. Therefore, we present new U-Pb and Pb-Pb zircon ages for key lithologies in the eastern part of the Variscan orogenic root, whose structural and metamorphic evolution is now well understood. The protolith and metamorphic ages of felsic rocks

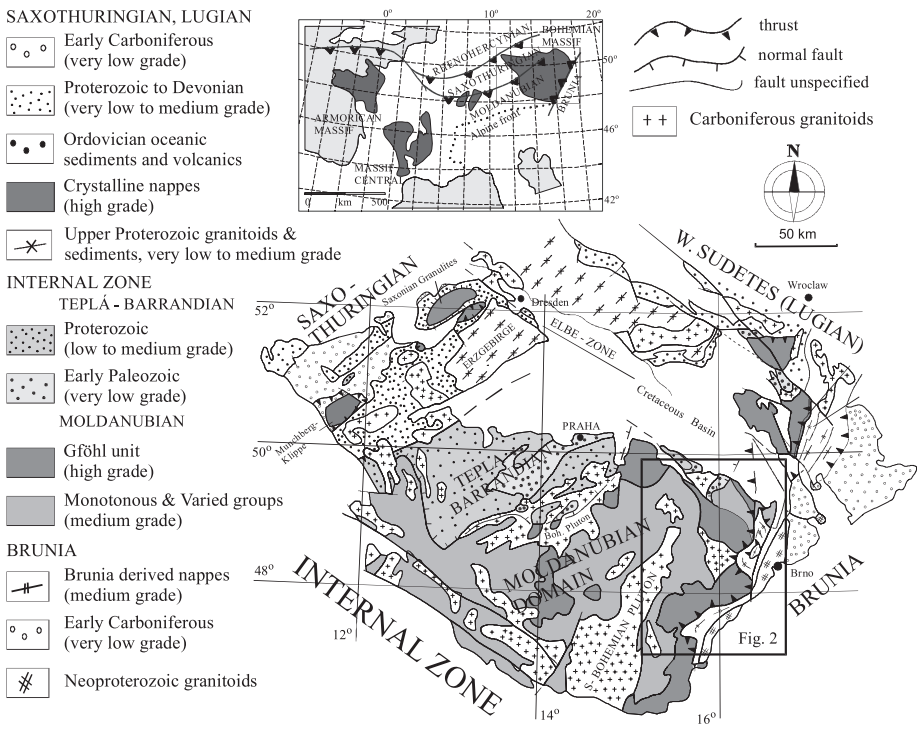

Fig. 1. Outline geological map of the eastern part of the Bohemian Massif with major units shown schematically. The location of the study area (fig. 2) is indicated. Upper left inset is the position of the study area within the framework of the European Variscides. (Modified after Franke, 2000.)

(essentially metavolcanic layers, granitoid orthogneisses, granulites and granitoids) were determined in order to establish a geodynamic framework including the pre- and syncollisional evolution of the eastern part of the Variscan orogen. Finally, from the present position of individual crustal units, we infer their different burial histories and the temporal evolution of crustal-scale buckling and syn-convergent exhumation of the deepest parts of the orogenic root, connected with lithospheric indentation of the Brunia foreland. The final increment of exhumation was dated by syntectonic intrusions associated with dextral wrenching along the NE-SW trending Brunia continental margin and the NW-SE oriented Elbe shear zone (fig. 1), thereby disrupting the orogenic fabric. Based on the new age data and existing paleomagnetic models we discuss the possible role of far-field forces on late exhumation processes within a hot orogenic root system.

GEOLOGY OF THE EASTERN MARGIN OF THE BOHEMIAN MASSIF

The eastern margin of the Bohemian Massif provides a detailed picture of its geological inventory as has already been recognized by Suess (1912, 1926). The eastern segment of the Brunia foreland is made up of unmetamorphosed and virtually undeformed Neoproterozoic granitoids (for example, Finger and others, 2000; Kröner and others, 2000b), which intruded into Neoproterozoic high-grade schists and migmatites (Fritz and others, 1996). This basement is unconformably overlain by Cambro-Ordovician clastic and pelitic metasediments, bimodal metavolcanic rocks, shallow marine Devonian sediments and Carboniferous foreland basin sediments (Hartley and Otava, 2001; Kalvoda and others, 2003). A NE-SW trending belt of

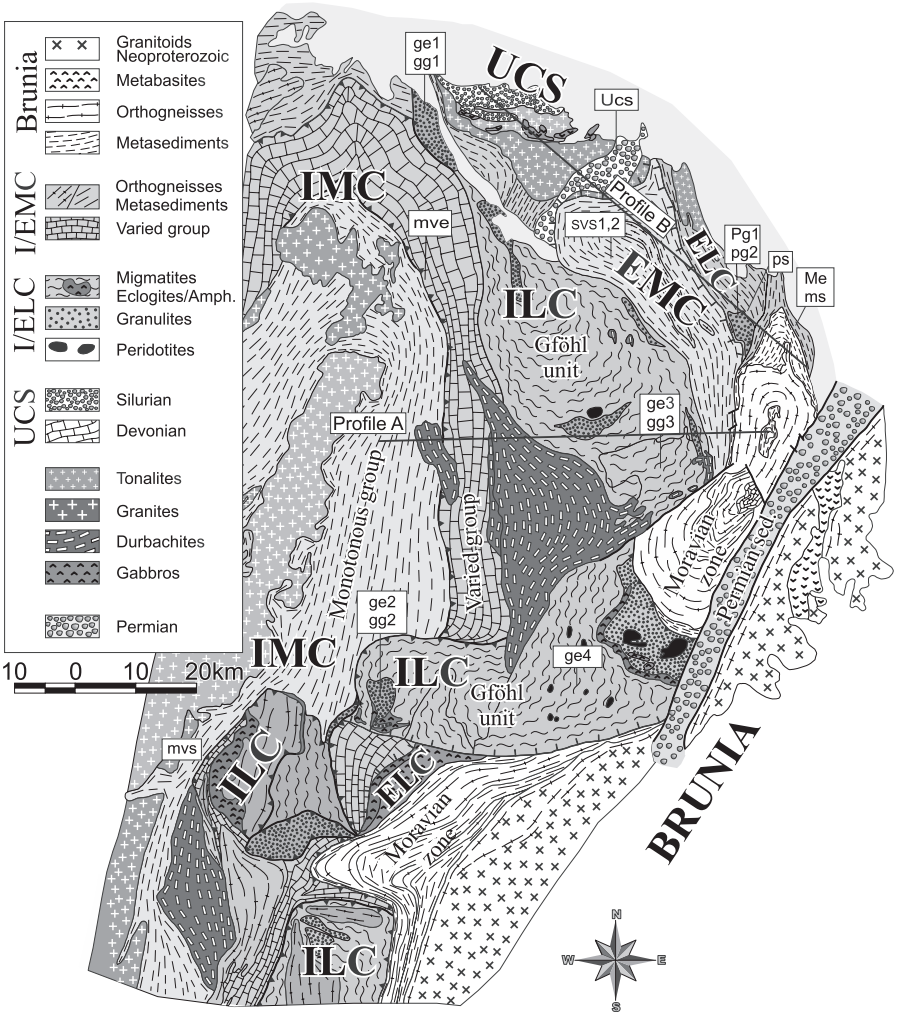

Fig. 2. Geological map of the eastern margin of the Bohemian Massif showing the distribution of crustal levels. Sample localities for geochronology are shown. Abbreviations: IMC – internal middle crustal belt; EMC – extrenal middle crustal belt; ILC – internal lower crustal belt; ELC – external lower crustal belt; UC – upper crustal segment; ge – Gföhl eclogite; gg – Gföhl granulite; ucs – upper crustal schists; svs – Svratka Unit schists; pg – Policka Unit granulites; ps – Policka Unit schists; me – Moravian Zone eclogites; ms – Moravian Zone schists; mve – Monotonous and Varied Units eclogites; mvs - schists of Monotonous and Varied Units. Positions of cross-sections A and B from figure 5 are marked by thick lines.

sheared and metamorphosed Brunia-derived rocks represents a zone of deformation along the western margin of the Brunia continent. This 300 km long and 50 km wide belt was named the Moravian zone in its southern part and consists of two NE-SW elongated tectonic windows emerging through high-grade rocks of the overlying Moldanubian domain: the southern Thaya window and northern Svratka window (fig. 2, Suess, 1926). The interface between the Moravian zone and the overthrust Moldanubian domain is marked by a narrow belt of kyanite-bearing micaschists interpreted as a major shear zone along which the high-grade Moldanubian gneisses and migmatites were retrogressed and thrust to the east (Moravian Micaschist Zone of Suess, 1912, 1926).

The Moldanubian domain (MD) east of Central Moldanubian pluton (fig. 1) has been subdivided into three major lithotectonic units that were previously identified and defined in Lower Austria (Thiele, 1976; Matura, 1984; Fuchs, 1986), namely the Monotonous Unit to the west and the Varied and Gföhl Units to the east, adjacent to the Moravian Zone (fig. 2). Tollmann (1982) grouped the Monotonous and Varied Units into the so-called Drosendorf terrane, based on their relatively low degree of metamorphism compared to the high-grade Gföhl Unit. This lithotectonic subdivision is valid for the entire Moldanubian domain in which the Monotonous Unit represents the structurally lowermost unit. It consists of K-feldspar-sillimanite±cordierite migmatitic paragneisses (metagraywacke) interlayered with leucocratic, K-feldspar-rich granitoid orthogneisses and rare eclogitic tectonic lenses (Dudek and Fediuková, 1974; O'Brien, 1997; O'Brien and Vrána, 1997). The Varied Unit occurs structurally above the Monotonous Unit, and their mutual contact is defined by uniformly deformed bodies of granitic gneiss (Fuchs and Matura, 1976). The Varied Unit consists of a strongly deformed, thick sequence of biotite-plagioclase gneisses with garnet, sillimanite and/or interlayered calc-silicate rocks, quartzite, intercalations of marble, graphite schists and numerous bodies of amphibolite. The Gföhl Unit is made up of a large body of granitoid gneiss associated with migmatites and K-feldspar-sillimanite paragneisses, locally accompanied by partially molten amphibolite bodies at its base. Today it represents the uppermost structural level of the Moldanubian zone and contains numerous bodies of Ky-Kfs granulite as well as tectonic lenses of eclogite and garnet and/or spinel peridotite. According to many authors the Gföhl Unit constitutes the highest part of the Moldanubian nappe pile, tectonically overlying the Drosendorf terrane (Fuchs, 1986; Franke, 1989; Matte and others, 1990).

P-T Evolution and Previous Geochronology of the Study Area

The NE-SW oriented Variscan structure of the eastern Bohemian Massif is intersected by the crustal-scale NW-SE trending Elbe Fault Zone (EFZ) that separates the northerly Sudetic realm from the main part of the Bohemian Massif (fig. 1). Our study area (fig. 2) covers the eastern part of the orogenic root between the EFZ to the north and the Moravian Zone on the east.

The basement granitoids of the Brunia continent in the study area yielded Neoproterozoic ages as documented by zircon as well as $^{40}Ar/^{39}Ar$ cooling ages (van Breemen and others, 1982; Fritz and others, 1996; Finger and others, 2000; table 1). These rocks and unconformably-overlying shallow marine Devonian metasediments show weak Variscan deformation and lower greenschist-facies metamorphism (Špaček and others, 2001; Franců and others, 2002). The metamorphic pattern of the Brunia-derived Svratka tectonic window shows a well-developed tectonically inverted Barrovian zonation ranging from the chlorite to sillimanite zone (Schulmann and others, 1991). The age of this metamorphism is Carboniferous on the basis of $^{40}Ar/^{39}Ar$ geochronology (Macintyre and others, 1992; Fritz and others, 1996; table 1).

In the north, high-grade rocks of the Gföhl Unit contain eclogite lenses with estimated minimum pressures of 18 to 19 kbar and temperatures of ~890 °C, surrounded by felsic granulite (Medaris and others, 1998; ge1 in figs. 2 and 3). Similar eclogites of the Gföhl Unit were overprinted at medium pressures of 9 to 12 kbar and temperatures of 750 to 850 °C (Kolenovská and others, 1999; ge2 in figs. 3 and 4). The common feature of these eclogite bodies is their basaltic composition and spatial association with felsic granulites, suggesting a crustal origin for these rocks (Medaris and others, 1998). Associated felsic granulites in the inner part of the Gföhl Unit reveal PT conditions of 825 to 840 °C at 11 to 17.5 kbar (Medaris and others, 1998; gg1 in figs. 3 and 4) and 800 to 850 °C at 9.5 to 11 kbar (Kolenovská and others, 1999; gg2 in figs. 3 and 4), the latter of which are considered to reflect conditions of re-equilibration. Granulites of the study area reveal temperatures of 840 °C at 18 to 19 kbar, re-

TABLE 1

List of published geochronological data from the studies area.

Unit	Rock type	Age	Method	Reference
Brunia domain				
Brno Massif	Metarhyolite	725 ± 15	Pb-Pb (zircon evapor.)	Finger and others (2000)
	Diorite	584 ± 5	U/Pb (zircon)	van Breemen and others (1982)
	Diorite	598.9 ± 1.0	Ar/Ar plateau (amphibole)	Fritz and others (1996)
	Diorite	586.9 ± 0.5	Ar/Ar plateau (amphibole)	
	Pegmatite	565.3 ± 0.8	Ar/Ar plateau (muscovite)	
Letovice Complex	Amphibolite	346 ± 3	Ar/Ar plateau (amphibole)	Macintyre and others (1992)
	Amphibolite	336 ± 5	Ar/Ar plateau (amphibole)	
	Amphibolite	343 ± 5	Ar/Ar plateau (amphibole)	
Thaya dome	Amphibolite	341 ± 2.2	Ar/Ar isotope corr. (amphibole)	Fritz and others (1996)
	Metagranite	582 ± 10	U/Pb (zircon)	Friedl and others (2004)
	Metagranite	566 ± 10	U/Pb (zircon)	
	Metagranite	568 ± 10	U/Pb (zircon)	
	Orthogneiss	1643 ± 10	Pb/Pb (zircon)-inherited core	
	Orthogneiss	595 ± 7	U/Pb (zircon)	
	Orthogneiss	581 ± 9	U/Pb (zircon)	
	Orthogneiss	589 ± 7	U/Pb (zircon)	
	Granite	551 ± 6	Rb/Sr whole rock isochron	Scharbert and Batík (1985)
	Orthogneiss	326.5 ± 0.4	Ar/Ar plateau (muscovite)	
	Amphibolite	341.1 ± 1.4	Ar/Ar isotope corr. (amphibole)	Dallmeyer and others (1992)
	Amphibolite	328.7 ± 3.3	Ar/Ar isotope corr. (amphibole)	
	Orthogneiss	325.5 ± 0.7	Ar/Ar isotope corr. (muscovite)	
	Orthogneiss	328.7 ± 0.8	Ar/Ar isotope corr. (muscovite)	
Svratka dome	Amphibolite	575.6 ± 2.2	Ar/Ar isotope corr. (amphibole)	Fritz and others (1996)
	Orthogneiss	326.5 ± 0.6	Ar/Ar plateau (muscovite)	
	Micaschist	330.0 ± 0.5	Ar/Ar plateau (muscovite)	

TABLE 1
(continued)

Unit	Rock type	Age	Method	Reference
ILC				
Raabs Complex	Orthogneiss	428 ± 6	U/Pb (zircon)	Finger and von Quadt (1995)
Strážek Complex	Granulite	347 ± 9	U/Pb (zircon)	Kröner and others (1998)
	Grt pyroxenite	373 ± 7	Sm/Nd (WR-mineral)	Brueckner and others (1991)
Gföhl Unit	Orthogneiss	493 ± 7	U/Pb (zircon)	Friedl and others (2004)
	Orthogneiss	484 ± 7	U/Pb (zircon)	
	Orthogneiss	478 ± 7	U/Pb (zircon)	
	Orthogneiss	474 ± 6	U/Pb (zircon)	
	Orthogneiss	433 ± 6	U/Pb (zircon)	
	Orthogneiss	335 ± 5	U/Pb (zircon)	
	Orthogneiss	334 ± 5	U/Pb (zircon)	
	Granulite	2336 ± 23	Pb/Pb (zircon)-inherited core	
	Granulite	446 ± 59	Pb/Pb (zircon)	
	Granulite	437 ± 9	U/Pb (zircon)	
	Granulite	433 ± 8	U/Pb (zircon)	
	Eclogite	324 ± 5	Sm/Nd (WR-mineral)	
	Eclogite	341 ± 7	Sm/Nd (WR-mineral)	
	Eclogite	323 ± 7	Sm/Nd (WR-mineral)	Beard and others (1992)
	Eclogite	336 ± 16	Sm/Nd (WR-mineral)	
	Eclogite	342 ± 9	Sm/Nd (WR-mineral)	
	Grt pyroxenite	343 ± 17	Sm/Nd (WR-mineral)	Medaris and others (1995)
	Eclogite	344 ± 6	Sm/Nd (WR-mineral)	

TABLE 1
(continued)

Unit	Rock type	Age	Method	Reference
IMC				
Variegated Unit	Metabasalt	358 ± 6	U/Pb (zircon)	Friedl and others (1993)
	Orthogneiss	2336 ± 23	Pb/Pb (zircon)-inherited core	Friedl and others (2004)
	Orthogneiss	621 ± 8	U/Pb (zircon)	
	Orthogneiss	622 ± 9	U/Pb (zircon)	
	Orthogneiss	618 ± 8	U/Pb (zircon)	
Southern Bohemian Batholith	Bt-granite	323 ± 4	U/Pb (monazite)	refs in Finger and others (1997)
		327 ± 5	U/Pb (monazite)	
		328 ± 5	U/Pb (monazite)	
	Granodiorite	328 ± 4	U/Pb (zircon)	
	Bt-granite	319 ± 6	U/Pb (monazite)	
	Ms-Bt-granite	327 ± 4	U/Pb (monazite)	
ELC				
Polička Complex	Orthogneiss	338 ± 3	U/Pb (monazite)	van Breemen and others (1982)

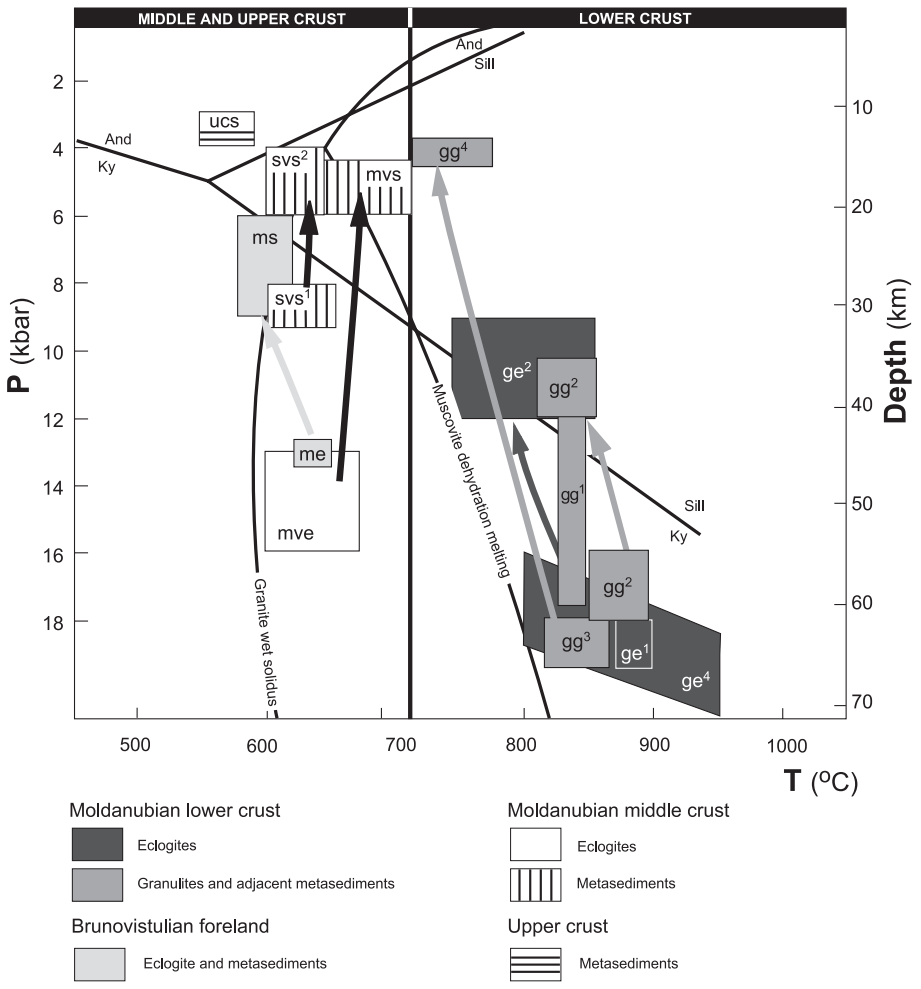

Fig. 3. Temperature-depth diagram showing P-T estimates for Variscan assemblages along the eastern margin of the Bohemian Massif and assuming lithostatic pressure (P = 1 ρgh). Dark gray boxes show peak (gg1, gg3, pg1) and re-equilibration (gg2, gg3, gg4, pg2) conditions for felsic ILC and ELC granulites (Medaris and others, 1998; Kolenovská and others, 1999; Schulmann and others, 1999; Tajčmanová and others, 2005). Black boxes show estimates of peak (ge1, ge3) and re-equilibration (ge2) stages for ILC eclogites by Medaris and others (1995a, 1998) and Kolenovská and others (1999). White box shows peak conditions for IMC eclogites (mve; Medaris and others, 1995a). Vertically hatched boxes show peak and re-equilibration conditions for IMC and EMC micaschists (mvs, svs1, svs2; Vrána, 1995; Pitra and Guiraud, 1996; Petrakakis, 1997). Light gray boxes show peak conditions for Brunia-derived eclogites and micaschists (me, ms; Konopásek and others, 2002). Horizontally hatched box shows peak conditions of UC (ucs; Pitra and others, 1994; Pitra and Guiraud, 1996). Reaction 1 – alumosilicate triple point, 2 – biotite dehydration melting, 3 – muscovite dehydration melting, 4 – pelite wet solidus, 5 – Alb = Jd+Qtz, 6 - Bio+Alb+Sil+Qtz → Grt +Crd+Kfsp+L (compiled by Thompson, 1999, 2000).

equilibrated at 760 to 800 °C and 10 to 13 kbar and later at 720 to 777 °C and 4 to 4.5 kbar (Tajčmanová and others, 2005; gg3 in figs. 3 and 4). The Gföhl Unit in the study area contains numerous tectonically emplaced bodies of garnet and spinel peridotite (T 900 – 1300 °C, P 28 – 44 kbar), associated with lenses of eclogite (T 800 – 950 °C, P 16 – 20 kbar) and clinopyroxenite, representing high-pressure partial melts of the upper mantle (Medaris and others, 1995a; Medaris, 1999; ge4 in figs. 3 and 4).

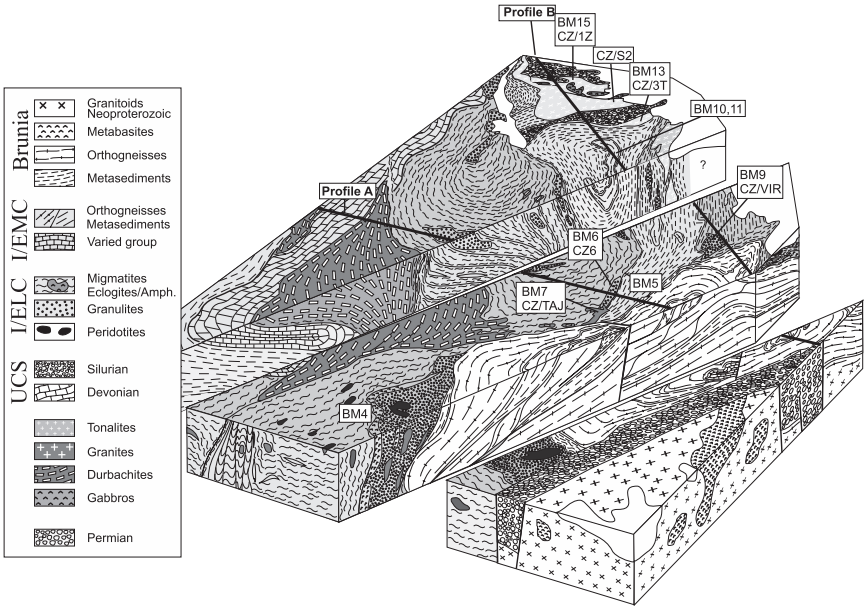

Fig. 4. Schematic block diagrams of three critical areas showing main structural features and orogenic fabric in the study area along NE-SW oriented sections. Intermediate block diagram shows tectonic style of imbrication of the Brunia foreland and overthrusting of the Moldanubian lower crust according to Schulmann and others (1991). Eastern block-diagram shows relationships between IMC (the Monotonous and Varied Units), ILC (the Gföhl Unit), EMC (The Svratka Crystalline Complex) and ELC (The Polička Unit) along a section perpendicular to the Elbe Shear Zone. Positions of cross-sections A and B from figure 5 are marked by thick lines. The scale is arbitrary.

Multigrain zircon and monazite fractions from granulites of the Gföhl Unit yielded U-Pb ages between 370 and 337 Ma (van Breemen and others, 1982; Kröner and others, 1988; table. 1). Eclogites of the same unit yielded Sm-Nd whole-rock-garnet ages ranging between 341 and 323 Ma, whereas associated peridotites show both Devonian and Carboniferous ages (Brueckner and others, 1991; Beard and others, 1992; Medaris and others, 1995b; table 1).

To the west, the Gföhl Unit is bordered by the Varied and Monotonous Units containing rare lenses of eclogite revealing minimum PT conditions of 600 to 680 °C at 13 to 16 kbar (Dudek and Fediuková, 1974; Medaris and others, 1995a, 1998; O'Brien, 1997; O'Brien and Vrána, 1997; mve in figs. 3 and 4). Metamorphic conditions in the surrounding gneisses yielded 600 to 720 °C at 4.5 to 6 kbar (Vrána, 1995; Petrakakis, 1997; mvs in fig. 4).

To the north and northeast, the Gföhl Unit is in contact with a medium-grade unit (Svratka Crystalline Complex), which lithologically resembles the Monotonous Unit and consists of garnet-sillimanite paragneisses interlayered with numerous bodies of porphyritic and fine-grained granitoid gneiss and migmatite. Kyanite-bearing paragneisses reveal peak P-T conditions of 8 to 9 kbar and 610 to 660 °C and re-equilibration conditions at 4 to 6 kbar and 600 to 650 °C in the sillimanite stability field (Pitra and Guiraud, 1996; svs1 and svs2 in figs. 3 and 4). $^{40}Ar/^{39}Ar$ dating indicates Carboniferous cooling ages of 325 to 332 Ma for samples of the Svratka Crystalline Complex (Fritz and others, 1996). The boundary between the high-grade Gföhl Unit and this medium-grade unit is marked by small-scale finger-like intrusions of K- and Mg-rich syenite (locally known as durbachite; Holub and others, 1997) that constitutes a large batholith within the Gföhl Unit farther to the south.

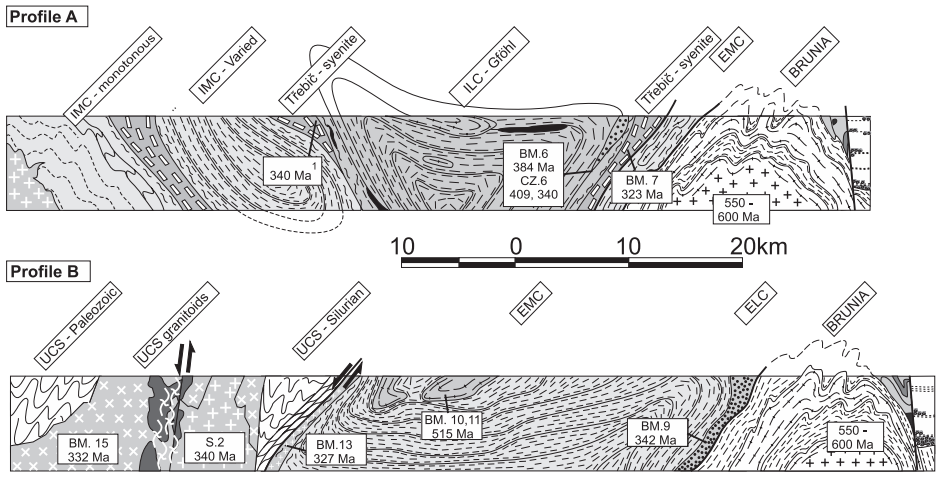

Fig. 5. Schematic sections across the eastern margin of the Bohemian Massif showing major structures, lithologies of individual domains and main tectonic boundaries. (A) NE-SW section from the ILC (the Gföhl Unit) in the west to the Brunia foreland to the east, (B) NW-SE section from the UC (Chrudim and Hlinsko Paleozoic) in the W, EMC (the Svratka Crystalline Complex) to the Brunia foreland to the east. Age data from Kröner and others (1988), van Breemen and others (1982) and Fritz and others (1996). Horizontal scale is shown, vertical scale is arbitrary.

To the north and east, the sillimanite schists and orthogneisses are bordered by the Polička Unit, composed of garnet-kyanite micaschists with intercalations of felsic granulite and partly anatectic amphibolite (Schulmann and others, 1999; pg1 and pg2, fig. 3). Monazites from one of these granulite bodies produced a multigrain U-Pb age of 338 ± 3 Ma (van Breemen and others, 1982). Farther south, this unit is strongly tectonically reduced and overlies a narrow strip of kyanite-bearing micaschists of the Moravian Micaschist Zone, rimming the entire eastern margin of Brunia-derived tectonic windows. Staurolite-bearing micaschists (580 – 620 °C, 6 – 9 kbar) of this belt also occur along the eastern flank of the Svratka window and contain eclogite boudins which exhibit minimum pressure conditions of 13 kbar at temperatures of 625 to 655 °C (Konopásek and others, 2002; ms, me in figs. 3 and 4).

A sequence of weakly metamorphosed Silurian to Devonian metasediments (the Paleozoic Hlinsko and Chrudim rocks) is separated by a major normal shear zone from the underlying NW- termination of the above-mentioned medium-grade unit of sillimanite para- and orthogneisses (Pitra and others, 1994; ucs in figs. 4 and 5). The NE-SW trending contact between these two units is marked by the sheet-like intrusion of a granodiorite sill. Intrusion of this sill was probably accompanied by metamorphism of Silurian metapelites at a pressure of ~4 kbar and temperatures of 550 to 590 °C (Pitra and others, 1994; Pitra and Guiraud, 1996).

Lithotectonic Zonation of the Moldanubian Orogenic Crust

The lithological content and inferred metamorphic conditions of the main units of the Moldanubian domain can be used to define a lithotectonic zonation that corresponds to crustal levels existing during maximum thickening of the orogenic root. The main reason for such a classification is to understand the spatial pattern of units that experienced different vertical displacement during exhumation. Interpretation of these units as syn-thickening crustal levels, their geometry and structural record may help to unravel mechanisms of exhumation and burial of these units. According to the lithological content and peak PT conditions described above, the Gföhl Unit can

be defined as a granulite-eclogite unit representing thickened crust that reached a depth of ~60 km and will be further described as *orogenic lower crust*. The granulite-bearing sillimanite paragneiss unit adjacent to the deformed margin of the Neoproterozoic Brunia foreland is considered to represent an *external orogenic lower crust* (ELC), whereas the main body of the Gföhl Unit represents an *internal orogenic lower crust* (ILC). The middle crustal sillimanite-paragneiss unit that is sandwiched between the ILC and ELC is defined here as an *external orogenic middle crust* (EMC), whereas the Monotonous and Varied Units in the west are defined as an *internal orogenic middle crust* (IMC). The Silurian and Devonian sediments in the NE part of the study area represent the uppermost, least metamorphosed sequence of the orogenic root and are defined here as an *upper orogenic crust* (UC), insignificantly buried during the Variscan orogeny. The Moravian nappe sequence exposed in the Svratka window represents a metamorphosed and imbricated part of the Neoproterozoic Brunia foreland.

Tectonic Evolution of the Eastern Part of the Bohemian Massif

The main features of the tectonic evolution along the eastern margin of the Variscan orogenic front in the Bohemian Massif are shown in figures 4 and 5. The study area exhibits the transition from a NE-SW-trending orogenic fabric adjacent to the Brunia foreland to a NW-SE trend parallel to the Elbe fault zone. This continuous curvature in orogenic trend was already recognized by Suess (1926), but its kinematic significance was not discussed and understood.

Several studies have documented that the Moldanubian root system was thrust over the Brunia foreland along a major dextral transpressional zone associated with northeastward imbrication of the basement and formation of the Moravian Zone (for example, Fritz and others, 1996). In the study area, the underthrust Brunia foreland formed a pile of internally imbricated basement- and cover-derived thrust sheets forming the so-called Svratka tectonic window (Suess, 1912; Schulmann and others, 1991; fig 4). Granulites, ultramafic rocks and eclogites of the ELC, associated with micaschists of the Moravian Zone, were thrust over the Brunia foreland, thereby forming klippen east of the Svratka tectonic window (eastern parts of cross-sections A and B, fig. 5; Konopásek and others, 2002). The entire internally imbricated system of lower crustal rocks and basement-derived sheets was refolded along large-scale upright folds during final E-W shortening (Schulmann and others, 1991). This folding also affected the Culmian foreland basin of Visean to early Namurian age, suggesting the age of latest shortening to be around 320 Ma (Hartley and Otava, 2001).

The EMC displays early west-verging compressive structures, strongly reworked by non-coaxial extensional deformation with a NW-SE oriented stretching axis parallel to the Elbe zone (Melka and others, 1992). The ILC was thrust over this unit in the south, whereas farther to the north the EMC occurs in the hanging wall of ILC high-pressure granulites and migmatites (Němec, 1968; see fig. 4). This is associated with a change in trend of both belts from NNE-SSW in the south to NW-SE and parallel to the Elbe zone farther north. The ILC shows multiple structures as follows: (1) An early, steep, N-S-striking foliation and isoclinal folds associated with high-pressure mineral assemblages in granulites are interpreted as a result of E-W compression at lower crustal levels (Schulmann and others, 1999; Tajčmanová and others, 2005). (2) A second, gently inclined thrust-related amphibolite-facies fabric is associated with partial melting at medium to low pressures (Tajčmanová and others, 2005). This secondary fabric is more penetrative in schists and migmatites and is generally associated with a NE-SW stretching lineation and kinematic criteria, suggesting top-to-the-NE thrusting (Schulmann and others, 1994). Finger-like durbachite bodies were emplaced syntectonically during this late thrusting event at several localities along the boundary between the ILC and EMC belts (fig. 4). The main body of durbachite masks the contact between metasediments of the Varied Unit of the IMC and the ILC to the west and the fabric of

high-grade rocks of the ILC (fig. 2). However, in general the medium-grade schists and marbles of the IMC occur in the footwall of west-dipping high-grade rocks and granulites of the ILC (fig. 4 and western part of cross-section A in fig. 5). The ILC rocks also exhibit a polyphase character of deformation marked by refolding of an early, steeply dipping metamorphic fabric into a flat-lying migmatitic fabric. The large-scale structure of the high-grade gneisses of the ILC exhibit a bivergent structural pattern (a positive flower structure), which is perturbed in the vicinity of the Elbe fault zone (cross-section A in fig. 5).

Paleozoic metasediments of the UC in the northeastern part of the study area (fig. 1) were refolded along kilometer-scale steep folds (NW part of cross-section B in fig. 5; Pitra and others, 1994). These rocks were intruded by granodiorites and tonalites of calc-alkaline affinity (Holub and others, 1997), showing steep magmatic to solid-state fabrics (Hrouda and others, 1999). These authors suggested syntectonic emplacement of the granitoids during regional folding and, therefore, their crystallization age may determine the age of main shortening of the upper crustal Silurian sediments. Melka and others (1992) and Pitra and others (1994) documented intense normal shearing which affected the entire central and western part of the EMC and also postdates shortening-related fabrics in the hanging wall Silurian metasediments of the studied upper crustal segment (cross-section B in fig. 5). This ductile shearing is parallel in strike to the Elbe Fault Zone and is compatible with top-to-the-NW normal movement (Synek and Oliveriová, 1993). A late granodiorite sill was syntectonically emplaced along the boundary between the EMC and UC and delineates the so-called Hlinsko detachment (Pitra and others, 1994). Steep normal shear zones are developed farther west in the UC and also affected rocks of the granodiorite-tonalite suite (NW part of the cross-section B in fig. 5). Late granites intruded during normal shearing and were emplaced at supracrustal levels between a tonalite intrusion to the east and unmetamorphosed Silurian sediments to the west (Hrouda and others, 1999). A normal solid-state shear zone was developed in the older tonalite, whereas in the late granite the fabric is magmatic to subsolidus-state.

RESULTS OF ZIRCON DATING

Gföhl Orthogneiss and Migmatite at the Boundary Between ILC and EMC

Anatectic and strongly deformed orthogneiss sample BM 4 was collected in the Rokytka valley close to the village of Biskupice (fig. 4). The rock is composed of recrystallized K-feldspar and plagioclase layers; quartz ribbons are strongly annealed, and garnet occurs in biotite-rich bands with abundant sillimanite. In the outcrop sampled, the orthogneiss locally passes into migmatite and contains pockets of granitic melt. Migmatitic gneiss sample BM 5 comes from the Loučka valley close to the village of Skryje (fig. 4). It contains a considerable amount of anatectic melt, layers of recrystallized K-feldspar, plagioclase, quartz, biotite and sillimanite. We interpret these two samples as representing originally porphyritic coarse-grained granite that was strongly deformed under high-grade conditions and partially melted.

Abraded ball-shaped cores of originally euhedral, brown, transparent zircon grains of Gföhl orthogneiss sample BM 4 and three small fractions of migmatite sample BM 5 containing clear to milky euhedral grains and needles with little rounding at their terminations were analyzed after vapor dissolution (table 2) and plot on a regression line (MSWD = 1.3) with intercept ages at 394 ± 6 and 1374 ± 36 Ma (fig. 6). The long-prismatic grain morphologies in both samples indicate a magmatic origin. We therefore consider the lower intercept age of 394 ± 6 Ma to most closely reflect the time of crystallization of the magmatic protolith, whereas the upper intercept reflects the mean age of the Mesoproterozoic source from which the original granite was derived.

TABLE 2

U-Pb isotopic analyses of Bohemian zircons after dissolution using HF vapor transfer

Sample	Zircon description	$^{206}Pb/^{204}Pb^{m}$	$^{206}Pb/^{238}U^{c}$	% error	$^{207}Pb/^{235}U^{c}$	% error	$^{207}Pb/^{206}Pb^{c}$	$^{206}Pb/^{238}U$ age [Ma]	$^{207}Pb/^{235}U^{c}$ age [Ma]	$^{207}Pb/^{206}Pb$ age [Ma]	Corr. coeff.
BM 1-1	Abraded, 15 euhedral, clear grains	297 ± 5	0.1181	0.57	1.0787	1.42	0.0662 ± 8	719.6 ±4.1	743.0± 10.6	815±25	0.542
BM 1-2	Abraded, 15 well rounded grains, milky to clear	198 ± 3	0.0753	0.32	0.6349	1.51	0.0611 ± 8	468.0±1.5	499.1± 7.5	644±30	0.495
BM 1-3	10 clear, euhedral, grains, 100-125 μm	168 ± 3	0.0584	0.98	0.4375	2.19	0.0543 ± 10	365.9±3.6	368.5± 8.1	383±42	0.549
BM 1-4	6 purple, euhedral, clear, grains, > 125 μm	135 ± 1	0.0641	0.52	0.4931	2.46	0.0558 ± 13	400.5±2.1	407.0± 10.0	445±50	0.465
BM 1-5	Abraded, 6 brown euhedral grains, 100-125 μm, well rounded after abrasion	717 ± 16	0.0577	0.84	0.4453	1.19	0.0559 ± 4	361.6±3.0	374.0±4.5	450±18	0.747
BM 1-6	Abraded, 8 euhedral, brown grains 100-125 μm. Well rounded after abrasion	801 ± 16	0.06	0.59	0.4548	0.96	0.0600 ± 4	375.6±2.2	380.6± 3.7	604±13	0.673
BM 1-7	14 clear, euhedral, grains, rounded at tips	516 ± 4	0.0595	0.66	0.4581	0.83	0.0558 ± 3	372.6±2.5	382.9± 3.2	445±11	0.811
BM 1-8	14 tiny, clear, euhedral grains	357 ± 4	0.0517	0.24	0.4304	0.55	0.0546 ± 3	325.0±0.8	363.5± 2.0	397±11	0.518
BM 1-9	1 brown, clear, stubby grain	576 ± 6	0.0773	0.94	0.6293	1.01	0.0590 ± 2	480.0±4.5	495.7± 5.0	568±8	0.939
BM 1-10	1 brown, euhedral, patchy grain	1052 ± 30	0.0543	2.19	0.4085	3.28	0.0545 ± 9	340.9±7.5	347.8± 11.4	394±39	0.773
BM 1-11	3 clear, stubby grains	335 ± 1	0.0513	0.51	0.5183	0.88	0.0733 ± 4	322.5±1.6	424.0± 3.7	1023±12	0.635
BM 1-12	2 long prismatic grains	247 ± 7	0.0439	0.65	0.3524	5.35	0.0583 ± 30	277.0±1.8	306.5± 16.4	540±112	0.081
BM 1-13	1 euhedral, grayish, zircon tip	807 ± 97	0.0478	1.23	0.3541	6.04	0.0537 ± 267	301.0±3.7	307.8± 18.6	362±112	0.216
BM 3-1	Abraded, 3 grains, clear, brown, stubby	1251 ± 33	0.1137	0.48	1.1446	0.71	0.0730 ± 4	694.2±3.3	774.7± 5.5	1014±10	0.731
BM 3-2	Abraded, 3 grains, clear, brown, prismatic	2892 ± 58	0.121	0.54	1.2903	0.59	0.0773 ± 2	736.3±4.0	841.4± 5.0	1129±4	0.926
BM 3-3	3 brown, stubby grains	2330 ± 47	0.0745	0.78	0.6325	0.82	0.0616 ± 2	463.2±3.6	497.7± 4.1	660±5	0.951
BM 3-4	8 prismatic clear, brown grains	1250 ± 13	0.0908	0.75	0.7601	0.96	0.0607 ± 4	560.3±4.2	574.1±5.5	630±13	0.781
BM 3-5	4 clear euhedral grains	2985 ± 60	0.0837	0.72	0.8854	0.9	0.0767 ± 4	518.2±3.7	643.9±5.8	1115±11	0.802
BM 3-6	Abraded, 4 rounded, pink, formerly prismatic grains	773 ± 31	0.0976	0.4	0.9706	0.57	0.0721 ± 3	600.3±2.4	688.8±3.9	990±8	0.74
BM 3-7	Abraded, 3 prismatic brown milky grains	1030 ± 13	0.0773	0.24	0.6174	1.13	0.0579 ± 6	480.0±1.2	488.2±5.5	526±23	0.474
BM 3-8	Abraded, 2 prismatic clear grains, slightly polished	684 ± 27	0.092	0.35	0.802	0.86	0.0633 ± 5	567.4±2.0	598.0±5.1	717±16	0.528
BM 4-1	Abraded, 5 clear, slender, pink still oval shaped grains	475 ± 8	0.1239	0.38	1.8354	0.61	0.1074 ± 5	753.0±2.9	1058.2±6.5	1756±8	0.67

TABLE 2
(continued)

Sample	Zircon description	$^{206}Pb/^{204}Pb^{m}$	$^{206}Pb/^{238}U^{c}$	% error	$^{207}Pb/^{235}U^{c}$	% error	$^{207}Pb/^{206}Pb^{c}$	$^{206}Pb/^{238}U$ age [Ma]	$^{207}Pb/^{235}U^{c}$ age [Ma]	$^{207}Pb/^{206}Pb$ age [Ma]	Corr. coeff.
BM 4-2	Abraded, 4 ball shaped brown transparent grains	287 ± 7	0.0986	0.27	0.9571	1.24	0.0704 ± 8	606.2±1.6	681.8±8.5	940±24	0.373
BM 4-3	Abraded, 4 ball shaped brown transparent grains	197 ± 2	0.1043	0.36	1.0459	1.33	0.0727 ± 9	639.6±2.3	726.8±9.7	1006±24	0.508
BM 5-1	8 clear grains, < 75 μm	729 ± 10	0.0604	0.58	0.4795	0.75	0.0576 ± 3	378.1±2.2	397.7±3.0	513±10	0.799
BM 5-2	7 clear, stubby grains	839 ± 6	0.0879	0.57	0.6955	0.64	0.0574 ± 2	543.1±3.1	536.1±3.4	505±6	0.904
BM 5-3	6 euhdral needles	630 ± 17	0.0649	0.6	0.4839	0.85	0.0540 ± 3	405.4±2.4	400.7±3.4	372±13	0.732
BM 5-4	9 tiny euhedral, clear needles	375 ± 8	0.0567	0.76	0.4199	1.84	0.0537 ± 8	355.5±2.7	356.0±6.6	359±36	0.526
BM 5-5	15 subrounded clear grains, <63 μm	412 ± 6	0.0641	0.44	0.5412	1.05	0.0612 ± 6	400.5±1.8	439.2±4.6	647±19	0.518
BM 5-6	8 euhedral clear grains, <63 μm	533 ± 14	0.068	0.86	0.5921	1.59	0.0632 ± 8	424.1±3.6	472.2±7.5	715±27	0.622
BM 5-7	8 prismatic grains, milky with rounded tips	274 ± 4	0.0656	0.37	0.5121	1.69	0.0566 ± 9	409.6±1.5	419.9±7.1	477±34	0.478
BM 5-8	Clear needles with rounded tips	245 ± 4	0.0659	0.37	0.5111	1.34	0.0563 ± 7	411.4±1.5	419.2±5.6	463±27	0.466
BM 6-1	4 irregulary shaped grains, clear with spots	476 ± 7	0.0587	0.73	0.4312	1.27	0.0533 ± 5	367.7±2.7	364.0±4.6	340±22	0.67
BM 6-2	3 short, prismatic, clear, stubby grains	219 ± 1	0.0605	0.59	0.4471	1.53	0.0536 ± 7	378.7±2.2	375.2±5.7	354±30	0.49
BM 6-3	4 well rounded, clear grains	747 ±12	0.0612	0.57	0.4569	0.89	0.0542 ± 4	382.9±2.2	382.1±3.4	378±15	0.68
BM 7-1	2 stubby slightly brown and clear grains	3140 ± 7	0.0645	0.74	0.4705	0.95	0.0529 ± 1	402.9±3.0	391.5±3.7	325±6	0.943
BM 7-2	1 brown, short prismatic, clear grain	3742 ± 144	0.0422	1.01	0.307	1.52	0.0527 ± 2	266.5±2.7	271.9±4.1	317±10	0.905
BM 7-3	1 tip of a clear pinkish grain	1586 ± 12	0.0439	0.52	0.32	0.87	0.0528 ± 2	277.0±1.4	281.9±2.5	321±9	0.776
BM 9-1	3 clear, stubby grains, <63 μm	800 ± 40	0.0493	0.9	0.3603	3.14	0.0532 ± 9	310.2±2.8	312.4±9.8	339±39	0.322
BM 9-2	2 clear, stubby grains	805 ± 16	0.0502	0.52	0.3609	1.28	0.0534 ± 4	315.7±1.6	312.9±4.0	344±18	0.357
BM 10-1	Abraded, 3 brown clear elongated grains	1576 ± 16	0.2141	0.41	3.1423	0.45	0.106 ± 2	1250.6±5.1	1443.1±6.5	1739±3	0.93
BM 10-2	Abraded, 6 tiny, small and clear grains	235 ± 6	0.0836	0.44	0.6755	3.19	0.0586 ± 17	517.6±2.3	524.1±16.7	554±65	0.581
BM 10-3	Abraded, 4 prismatic, clear grains	467 ± 11	0.0893	0.73	0.8041	1.48	0.0653 ± 8	551.4±4.0	599.1±8.9	784±25	0.59
BM 10-4	Abraded, 5 well rounded clear grains	212 ± 3	0.1069	0.61	1.1031	1.84	0.0748 ± 12	654.7±4.0	754.8±13.9	1064±32	0.516
BM 11-1	Abraded, 1 prismatic clear grain	215 ± 2	0.0669	0.39	0.5209	1.48	0.0565 ± 8	417.5±1.6	425.8±6.3	471±29	0.463

TABLE 2
(continued)

Sample	Zircon description	$^{206}Pb/^{204}Pb^{m}$	$^{206}Pb/^{238}U^{c}$	% error	$^{207}Pb/^{235}U^{c}$	% error	$^{207}Pb/^{206}Pb^{c}$	$^{206}Pb/^{238}U$ age [Ma]	$^{207}Pb/^{235}U^{c}$ age [Ma]	$^{207}Pb/^{206}Pb$ age [Ma]	Corr. coeff.
BM 12-1	6 clear, irregular shaped grains, >100 μm	376 ± 5	0.0647	0.33	0.5074	1.01	0.0568 ± 5	404.1±1.3	416.7±4.2	486±20	0.485
BM 12-2	8 clear, euhedral grains, >100 μm	716 ± 9	0.0679	0.33	0.5182	0.66	0.0554 ± 3	423.5±1.4	423.9±2.8	428±12	0.572
BM 12-3	6 clear, pinkish euhedral grains, > 100 μm	850 ± 42	0.0586	0.65	0.5554	0.87	0.0688 ± 4	367.1±2.4	448.5±3.9	892±11	0.781
BM 12-4	7 clear, stubby grains, > 63-100 μm	464 ± 6	0.0642	0.67	0.4707	1.13	0.0532 ± 5	401.1±2.7	391.7±4.4	338±20	0.641
BM 13-1	6 brownish, euhedral grains with cracks	845 ± 5	0.05	0.26	0.365	0.39	0.0529 ± 1	314.5±0.8	315.9±1.2	326±6	0.688
BM 13-2	5 clear, euhedral grains, rounded tips	208 ± 1	0.0519	0.26	0.3791	1.49	0.0533 ± 5	326.2±0.8	326.4±4.9	344±22	0.446
BM 13-3	5 pink, euhedral clear grains	147 ± 1	0.0592	0.27	0.4354	1.05	0.0529 ± 7	370.8±1.0	367.0±3.9	326±32	0.466
BM 14-1	Abraded, 10 prismatic grains, rounded tips	216 ± 3	0.0549	0.44	0.3896	1.84	0.0514 ± 9	344.5±1.5	334.1±6.1	284±54	0.441
BM 14-2	3 stubby to euhedral, clear, grains	564 ± 23	0.0516	0.42	0.3698	2.51	0.0520 ± 12	324.3±1.4	319.5±8.0	305±17	0.428
BM 15-1	Abraded, 2 brown, elongated grains	818 ± 18	0.0556	0.34	0.4018	0.85	0.0524 ± 4	348.8±1.2	343.0±2.9	330±17	0.513
BM 15-2	Abraded, 7 prismatic, pink grains	294 ± 2	0.0555	0.32	0.4063	1.01	0.0530 ± 5	348.2±1.1	346.2±3.5	330±21	0.451
BM 15-3	Abraded, 10 clear well rounded grains. Formerly euhedral grains	280 ± 5	0.0614	0.47	0.4576	1.99	0.0540 ± 10	384.1±1.8	382.6±7.6	373±41	0.463

m = measured ratio; c = ratio corrected for common lead (Stacey and Kramers, 1975), spike, mass fractionation, and blank. All errors are 2 sigma.

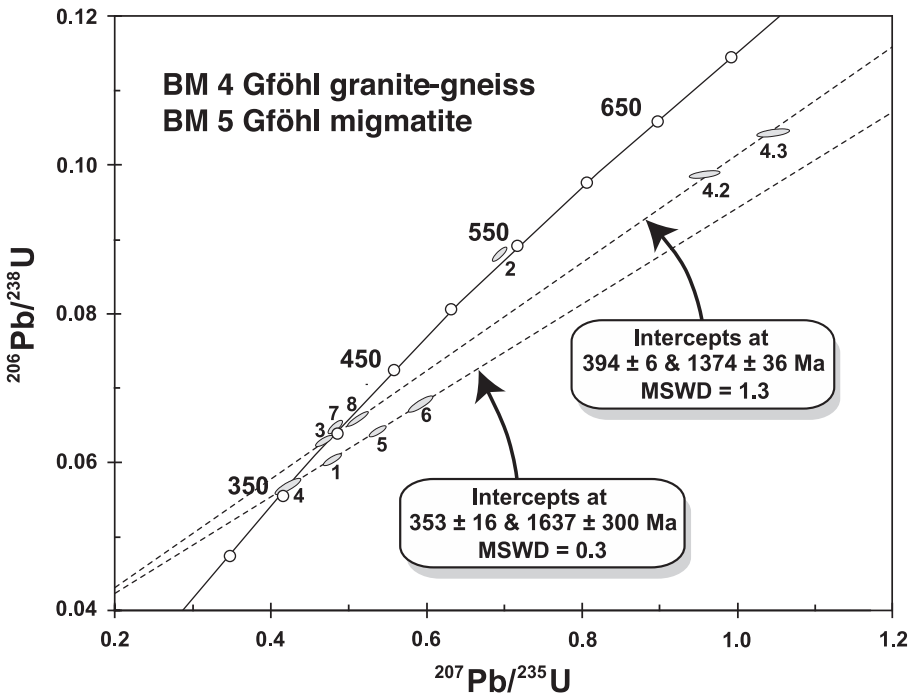

Fig. 6. Concordia diagram showing analytical data for zircons from Gföhl granitic gneiss sample BM 4 and migmatitic gneiss sample BM 5. Error ellipses are 2-sigma.

A distinctly different population of clear, stubby zircons in the same samples with variable degrees of partial dissolution at the originally pyramidal terminations as well as thin, euhedral and needle-like grains probably represent new zircon growth during advanced migmatization and partial anatexis. Several fractions of the stubby grains are discordant, whereas the clear needles are nearly concordant. All fractions are aligned along a chord (MSWD = 2.3), yielding a significantly younger lower intercept age of 353f ± 16 Ma and a poorly constrained upper intercept at 1637 ± 300 Ma (fig. 6). We interpret the younger age to reflect zircon crystallization during partial melting, whereas the upper intercept age of ~1637 Ma appears to reflect a similar crustal source as in the older zircon population.

A sample of least deformed, non-migmatitic Gföhl gneiss (CZ 14/4) was collected at locality Biskupice, 2 km east of sample BM 4, and is petrographically similar to BM 4. The homogeneous zircon population consists of long-prismatic grains, little rounded at their terminations, and clearly of igneous origin. Five grains were evaporated individually and yielded similar $^{207}Pb/^{206}Pb$ ratios that combine to a mean age of 550.6 ± 1.0 Ma (table 3, fig. 7A). This is likely to reflect the time of igneous emplacement of the gneiss precursor. Two similar looking zircons yielded significantly higher ages of 791.5 ± 2.8 Ma and 848.2 ± 2.9 Ma respectively (table 3, figs. 7B, C) and are interpreted as xenocrysts. The difference in age as compared to samples BM 4 and 5 and the lack of much older xenocrysts suggest that sample CZ 14/4 represents a distinct gneiss unit within the Gföhl assemblage and supports the assumption that the term "Gföhl gneiss" may include a variety of orthogneisses of different ages and origins.

TABLE 3

Pb isotopic data from single grain zircon evaporation.

Sample Number	Zircon color and morphology	Grain #	Mass scans[1]	Evaporation temp. in °C	Mean $^{207}Pb/^{206}Pb$ ratio[2] and 2-σm error	$^{207}Pb/^{206}Pb$ age and error
CZ 14/4	yellow-brown, long-prismatic, slightly rounded terminations	1	114	1596	0.058547±29	550.3±1.1
		2	62	1595	0.058564±61	550.9±2-3
		3	87	1589	0.058541±37	550.1±1.4
		4	127	1594	0.058566±22	550.1±0.8
		5	122	1596	0.058556±22	550.6±0.8
mean of 5 grains		1-5	512		0.058555±14	***550.6±1.0**
	yellow-brown, ends well rounded	6	83	1599	0.065534±88	791.5±2.8
		7	110	1598	0.067335±92	848.2±2.9
CZ-1Z	clear to light brown, stubby to long-prismatic, euhedral	1	110	1599	0.053072±46	331.9±2.0
		2	88	1600	0.053082±49	332.3±2.1
		3	66	1598	0.053091±58	332.7±2.5
mean of 3 grains		1-3	264		0.053080±29	332.2**±1.2**
2S	yellow-brown, long-prismatic, euhedral	1	87	1599	0.053267±33	340.2±1.4
		2	84	1600	0.053252±33	339.5±1.4
		3	122	1598	0.053271±29	340.4±1.2
mean of 3 grains		1-3	293		0.053264±18	***340.1±1.1**
CZ-3T	clear to yellowish-brown, long-prismatic, euhedral	1	81	1598	0.053017±37	329.5±1.6
		2	95	1597	0.053012±32	329.3±1.4
		3	94	1599	0.053046±24	330.8±1.0
mean of 3 grains		1-3	187		0.053025±18	***329.9±1.1**
CZ/TAJ	brown, long-prismatic, idiomorphic	1	106	1595	0.052869±38	323.2±1.6
		2	84	1594	0.052884±39	323.8±1.7
		3	103	1592	0.052874±30	323.4±1.3
		4	103	1594	0.052888±40	324.0±1.7
		5	63	1596	0.052881±29	323.7±1.2
		6	88	1595	0.052877±33	323.5±1.4
mean of 6 grains		1-5	547		0.052877±15	***323.5±1.1**
CZ 6	clear, near-spherical, multifaceted	1	133	1605	0.053264±23	340.1±1.0
		2	100	1604	0.053268±23	340.2±1.0
		3	99	1607	0.053254±27	339.6±1.2
		4	121	1602	0.053273±24	340.4±1.0
		5	107	1610	0.053259±19	339.8±0.8
		6	129	1609	0.053260±13	339.9±0.5
mean of 6 grains		1-6	689		0.053263± 9	***340.0±1.1**
		7	44	1596	0.054926±61	409.2±2.5
		8	98	1598	0.054323±25	384.5±1.0
		9	83	1597	0.054331±27	384.8±1.1
mean of 2 grains		8&9	181		0.0543	***384.6±1.1**
CZ/Vir	clear to yellowish-brown, long-prismatic, euhedral	1	89	1598	0.053227±35	338.5±1.5
		2	97	1597	0.053256±33	339.7±1.4
		3	68	1599	0.053238±46	339.0±2.0
mean of 3 grains		1-3	254		0.053241±21	***339.1±1.1**

[1]Number of $^{207}Pb/^{206}Pb$ ratios evaluated for age assessment. [2]Observed mean ratio corrected for nonradiogenic Pb where necessary. Errors based on uncertainties in counting statistics. *Error based on reproducibility of internal standard.

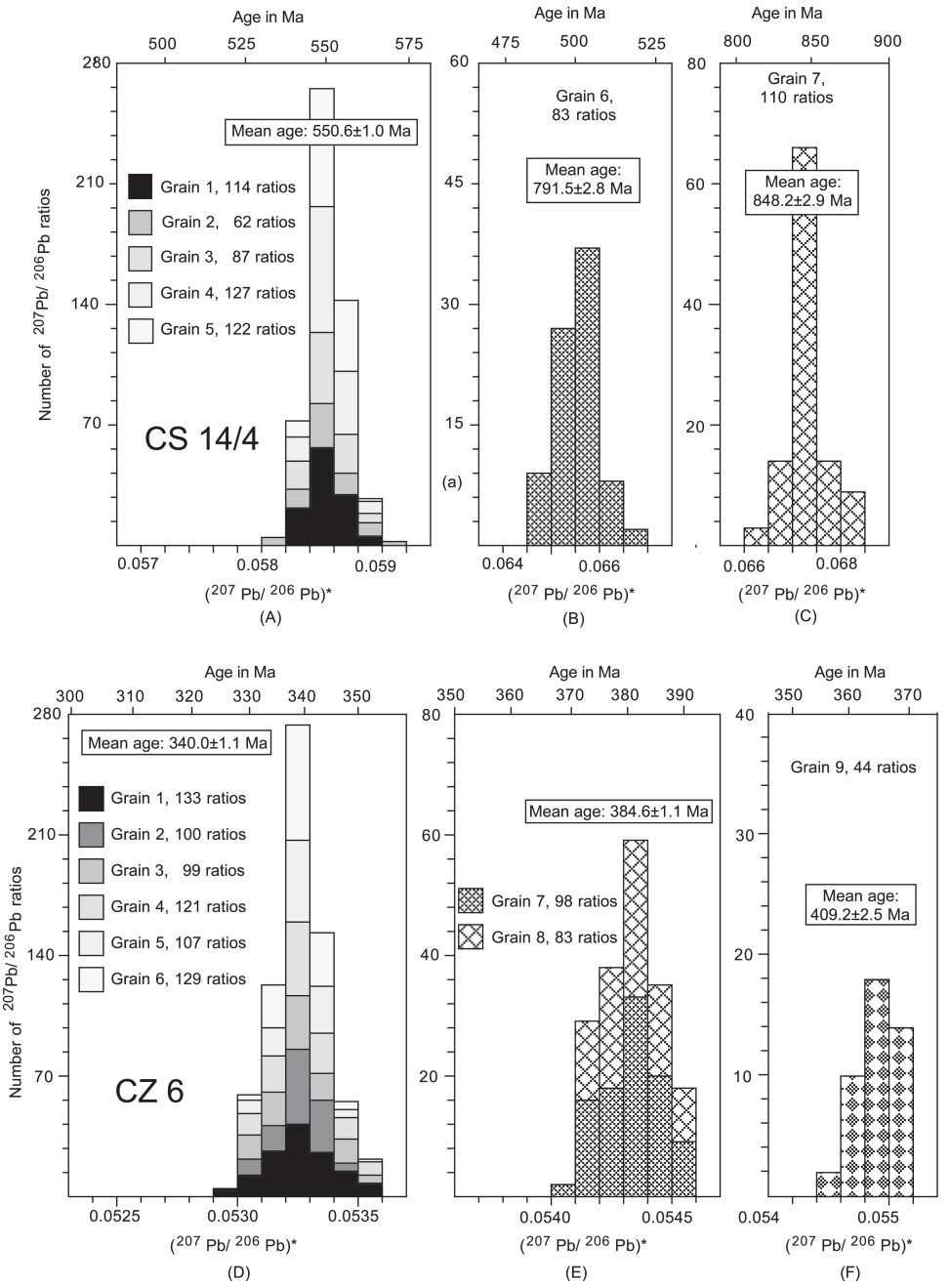

Fig. 7. Histograms showing distribution of radiogenic lead isotope ratios derived from evaporation of single zircons from rocks of the Variscan root zone, southern Bohemia, Czech Republic. (A) Spectrum for 5 grains from porphyritic granite-gneiss sample CZ 14/4, integrated from 512 ratios and interpreted to reflect age of protolith emplacement. (B, C) Spectra for xenocrystic grains. (D) Spectrum for 6 grain fractions of 3-4 metamorphic zircons each from granulite sample CZ 6, integrated from 689 ratios and interpreted to reflect age of high-grade metamorphism. (E) Spectrum for 2 igneous grains, integrated from 181 ratios and interpreted to reflect emplacement of granulite protolith. (F) Xenocrystic grain.

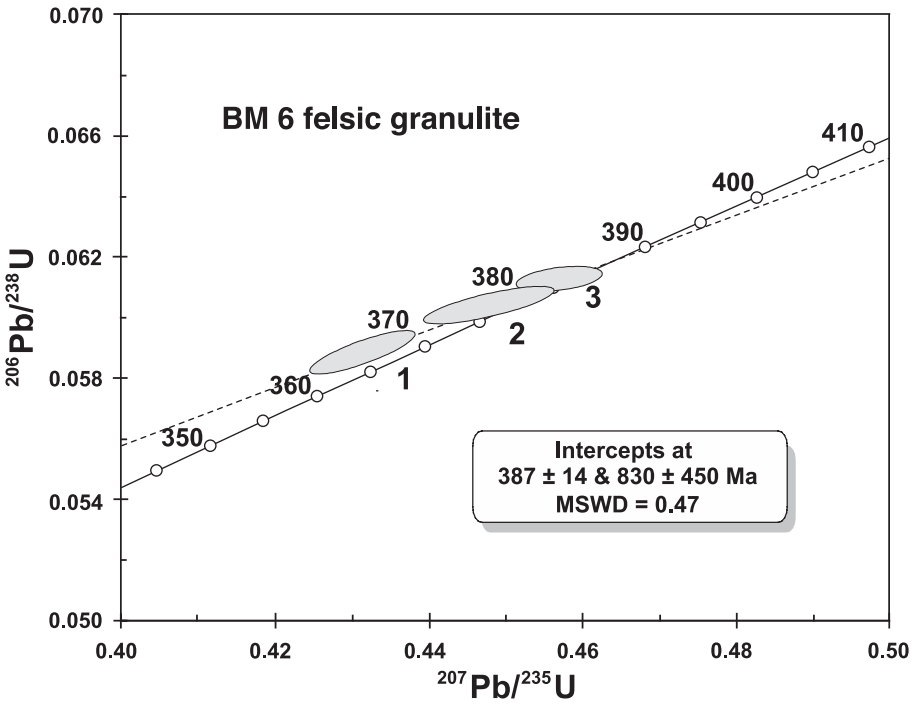

Fig. 8. Concordia diagram showing analytical data for zircons from felsic granulite sample BM 6. Errors as in figure 6.

Felsic Granulite Close to the Contact Between ILC and EMC

Felsic granulite sample BM 6 comes from the least retrograded portion of a granulite body in the Loučka Valley of the Drahonín area, close to the border between the Gföhl and Svratka crystalline units (fig. 4). The granulites in this area contain two contrasting metamorphic assemblages. The early assemblage is characterized by kyanite + garnet + biotite + plagioclase + quartz + mesoperthite, whereas the later assemblage contains sillimanite + garnet + spinel + biotite.

Sample BM 6 contains clear, oval-shaped and stubby zircons as well as irregularly-shaped grains with no internal zoning as is common in high-grade rocks. Six small fractions containing two to four grains each are slightly reversely discordant, presumably due to U-loss in the internal domains of the grain (Williams and others, 1984) or due to laboratory procedures, but plot near the concordia curve (fig. 8). Two oval-shaped grains of fraction 3 are 45 percent discordant and yielded an intercept age of 383 ± 3 Ma. The U-Pb data obtained from cores of clear, stubby and oval-shaped grains of fractions 5 and 6 are also reversely discordant but are well aligned (MSWD = 0.22) and, together with the remaining four fractions of oval-shaped grains, project to a concordia intercept age of 387 ± 14 Ma (table 2, fig. 8). Early Neoproterozoic inheritance is revealed by an ill-defined upper intercept age of 803 ± 450 Ma. The high degree of concordance of the abraded zircons makes it unlikely that these grains contain considerable amounts of older material, and we therefore interpret the age of 387 ± 14 Ma to reflect the time of crystallization of the granulite precursor. Wendt and others (1994) reported similar U-Pb zircon protolith emplacement ages of 365 to 373 Ma for South Bohemian granulites from the Blanský les massif.

An additional sample of felsic granulite was collected from the same locality (CZ 6) and contained abundant ball-shaped, clear, multifaceted zircons of metamorphic origin as well as clear to yellowish long-prismatic grains with well rounded terminations which appear to be of igneous derivation. Six small fractions of 3 to 4 grains each (~60 – 90 μm in diameter) of the metamorphic population were evaporated individually at high temperatures and yielded consistent $^{207}Pb/^{206}Pb$ ratios corresponding to a mean age of 340.0 ± 1.1 Ma (table 3, fig. 7D). This age is identical to metamorphic ages obtained from numerous granulite samples throughout the Bohemian Massif and reflects the peak of HP/HT metamorphism (Kröner and others, 2000a).

In contrast, the rounded, long-prismatic grains provided variable results. Two grains yielded similar isotopic ratios with a mean age of 384.6 ± 1.1 Ma, whereas one grain has a $^{207}Pb/^{206}Pb$ minimum age of 409.2 ± 2.5 Ma (table 3, figs. 7E, F). The former result is identical to the lower intercept age obtained by the vapor transfer method and, in our view, reflects the time of crystallization of the granulite precursor. The most plausible interpretation for the older age of ~409 Ma is mixing of the ~385 Ma magmatic components with an older source (core?) as reflected by the upper concordia intercept of the vapor transfer data (fig. 8). The "age" is therefore considered to be geologically meaningless.

Mg-K Syenite (Durbachite) Emplaced at the ILC and EMC Boundary

Sample BM 7 of dark porphyritic durbachite was collected close to the village of Drahonín (fig. 4) and is composed of K-feldspar phenocrysts, biotite, actinolitic hornblende, quartz and rare plagioclase.

The zircon population comprises short-prismatic and euhedral, clear to pink grains with no rounding at the ends. Two single grains and a micro-fraction of two stubby grains were analyzed by the vapor transfer method. The U-Pb data can be fitted to a regression line (MSWD = 0.43) through the origin and with an upper concordia intercept corresponding to an age of 323 ± 7 Ma (fig. 9). In view of the igneous nature of the zircons this is interpreted to date the time of emplacement of the durbachite.

Long-prismatic, euhedral single zircons from a second durbachite sample (CZ/TAJ) and collected from the same locality were evaporated and yielded a mean $^{207}Pb/^{206}Pb$ age of 323.5 ± 1.1 Ma (table 3, fig. 9, inset). This result is identical, but more precise, than the vapor transfer result and places a younger age limit on the steep fabric in the Gföhl granulites.

Granitic Gneisses from the EMC

Strongly deformed and recrystallized Svratka granitic augen-gneiss sample BM 10 was collected close to the village of Sněžná north of the town of Nové Město (fig. 4). The rock is composed of K-feldspar augens, recrystallized plagioclase, quartz ribbons as well as muscovite and biotite aggregates. The augen-gneiss is surrounded by sillimanite micaschists with a sillimanite + biotite + garnet + muscovite + plagioclase + quartz assemblage. Microgranite gneiss sample BM 11 was also collected close to the village of Sněžná and represents a typical example of the SCC, similar to augen-gneiss BM 10. It shows a strong planar fabric reflecting intense solid-state deformation and is composed of recrystallized K-feldspar, plagioclase and quartz. Muscovite is abundant, whereas biotite is rare.

Zircons from sample BM 10 are mostly subhedral and clear, transparent to light brown and translucent. Four small fractions of 3 to 6 morphologically identical grains each were treated in an air abrasion cell to remove potential metamorphic overgrowths. The grains of fraction 3 were only slightly abraded and thus at least partly kept their original, euhedral shape. The remaining fractions 1, 2 and 4 consisted of well-rounded, oval grains after abrasion, and the analytical data (table 2) show considerable dispersion in the Concordia diagram (fig. 10). Regression through all

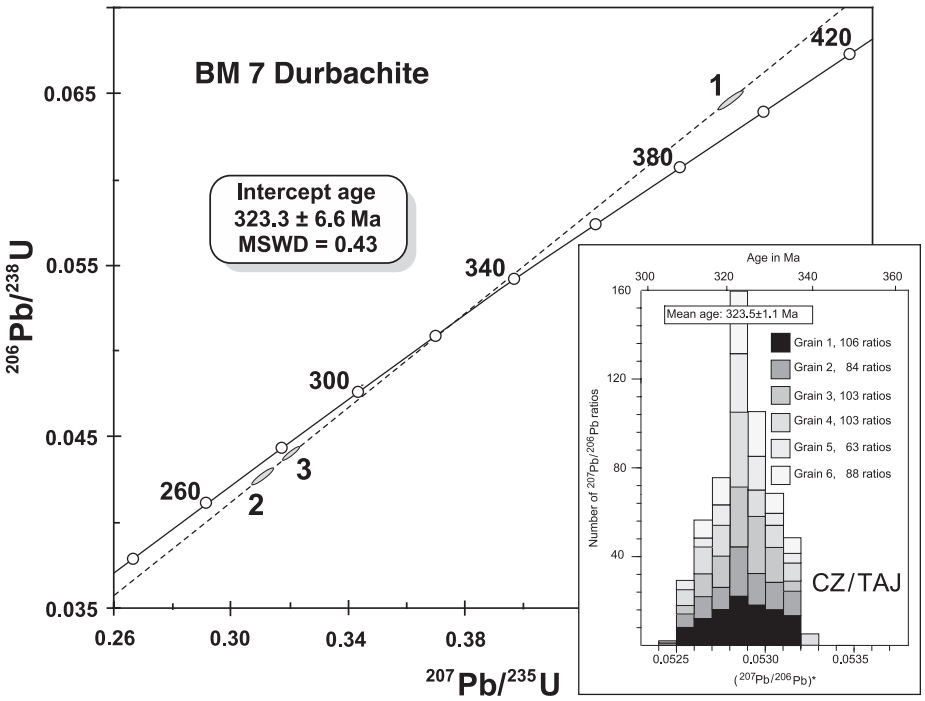

Fig. 9. Concordia diagram showing analytical data for zircons from porphyritic durbachite sample BM 7. Inset is histogram showing distribution of radiogenic lead isotope ratios derived from evaporation of 6 zircon grains from durbachite sample CZ/TAJ, integrated from 547 ratios.

four poorly aligned data points (MSWD = 5.6) yielded intercept ages of 508 ± 30 and 1927 ± 60 Ma. If the result for slightly abraded fraction 3 is excluded from the regression calculation, the MSWD significantly improves to 1.4, and the resulting discordia line yields statistically equivalent but better constrained intercept ages of 515 ± 9 and 1932 ± 7 Ma (fig. 10). The fact that the slightly polished grains plot below the 515 Ma discordia either suggests Pb-loss during high-grade metamorphism at ~340 Ma or metamorphic overgrowth at 340 Ma, or both. The age of 515 ± 9 Ma is thus interpreted to approximate the time of protolith emplacement, whereas the upper intercept age of 1932 ± 7 Ma suggests that the gneiss protolith resulted from melting of late Paleoproterozoic basement.

A single, elongate and abraded zircon grain was analyzed from microgranite-gneiss sample BM 11 (table 2), and the results plot well below the 515 Ma discordia for sample BM 10 (fig. 10). The corresponding $^{207}Pb/^{206}Pb$ minimum age of 471 ± 29 Ma is considered to reflect Pb-loss at an unspecified time in the past, and the result is therefore difficult to interpret. We shall therefore not consider this sample in the following discussion.

Melt Patch from Migmatitic Metabasite of the ELC

Sample BM 9 represents melt patches within amphibolites associated with the Vír granulite body and sampled in a quarry north of the village of Vír (fig. 4). Adjacent granulites exhibit a homogeneously developed high-grade metamorphic fabric related to severe retrogression and partial melting. The melt patches occur in neck zones of intrafolial boudin necks in lock-up shear bands. The rock is composed of a hbl-plg-

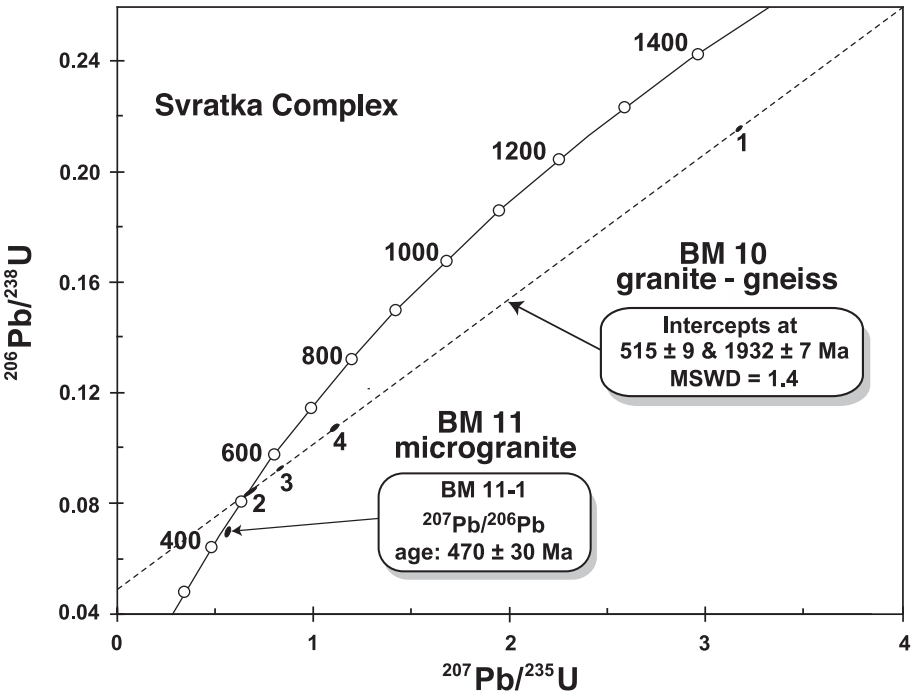

Fig. 10. Concordia diagram showing U-Pb zircon data for Svratka orthogneiss samples BM 10 and BM 11. Errors as in figure 6.

titanite assemblage, and the surrounding amphibolite is characterized by the assemblage hbl-plg-qtz±grt±cpx. The melt patches are interpreted as the result of *in-situ* melting of high-grade amphibolite.

The zircon population consists of clear, short prismatic to stubby grains, whereas milky-gray (metamict) grains are rare. Two fractions of two grains each and three transparent, stubby grains were analyzed after vapor transfer and provided slightly discordant isotopic ratios (table 2, fig. 11) and $^{207}Pb/^{206}Pb$ ages of 339 ± 39 and 344 ± 18 Ma with a mean of 341.6 ± 6 Ma (fig. 11) that we interpret to reflect the formation of melt patches in the Vír granulite body. Due to the slight discordance, the $^{206}Pb/^{238}U$ apparent age of this sample is distinctly younger at 310 Ma.

Zircons from a further sample of coarse-grained melt patch from the same locality (CZ/Vír) were clear to yellowish-brown, long-prismatic and euhedral. Evaporation of three large grains produced identical isotopic ratios that combine to a mean $^{207}Pb/^{206}Pb$ age of 339.1 ± 1.1 Ma (table 3, fig. 11, inset). This is identical to, but more precise than, the conventional $^{207}Pb/^{206}Pb$ age and is considered to be the best estimates for the time of melt patch formation.

Granodiorite Sill Emplaced at the Boundary Between EMC and UC

Strongly sheared granodioritic gneiss sample BM 13 was collected from a sill near the village of Krouna in the Krouna River valley (fig. 4). The sill was affected by solid state normal shearing marked by a strong NW-SE trending stretching lineation, but granodiorite veins cross-cut the main fabric and indicate a syntectonic origin for the intrusion (Pitra and others, 1994). The rock contains relict plagioclase porphyroclasts, locally strongly recrystallized, recrystallized biotite, amphibole and quartz.

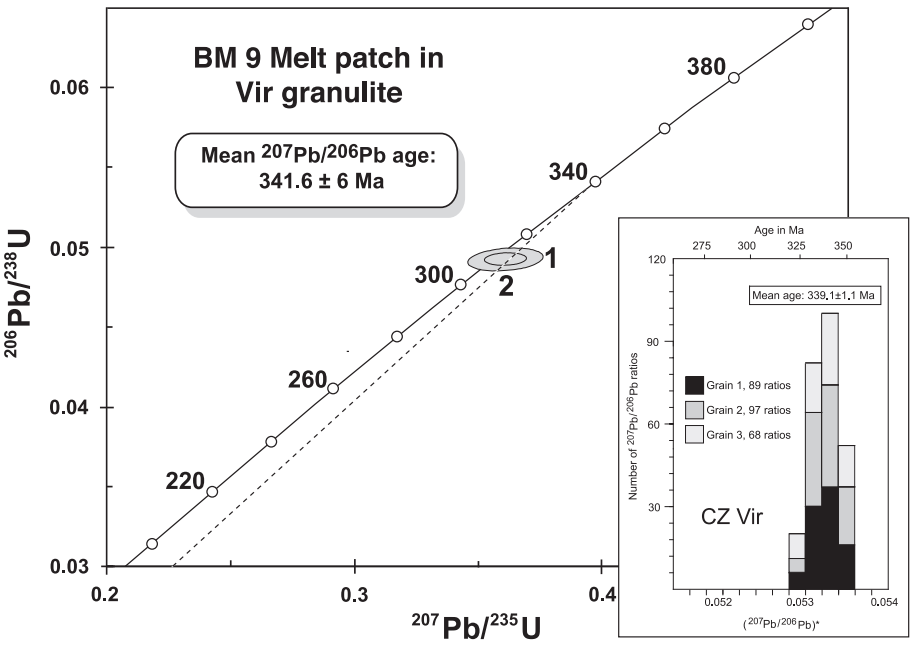

Fig. 11. Concordia diagram showing U-Pb zircon data for meltpatch sample BM 9 within amphibolites of the Vír granulite. Inset is histogram showing distribution of radiogenic lead isotope ratios derived from evaporation of 3 zircon grains from granulite sample CZ/Vir, integrated from 254 ratios.

The zircons are brownish to clear and predominantly euhedral, but there are also grains with slightly rounded terminations. The analytical results after vapor transfer dissolution of three fractions containing 5 to 6 grains each are presented in table 2 and figure 12. Euhedral grains with cracks (fraction 1) document recent Pb-loss and, together with two additional fractions of euhedral grains, one concordant and one grossly reversely discordant, can be fitted to a regression line (MSWD = 1.3) from the origin to an upper intercept age of 327 ± 6 Ma (fig. 12). This is considered to reflect the time of emplacement of the gneiss protolith.

The additional sample CZ/3T was collected from the same locality as BM 13, and individual evaporation of three euhedral zircon grains yielded consistent $^{207}Pb/^{206}Pb$ ratios with a mean age of 323.5 ± 1.1 (table 3, fig. 12, inset). This is identical to, but more precise than, the vapor transfer data and provides a well-constrained older age limit for the shearing event.

Granitoids Emplaced into the Upper Crust

This plutonic complex consists of two major intrusive phases, namely an older amphibole-bearing granodiorite (sample CZ/2S) and younger pink granite (sample BM 15) representing a shallow intrusion of subvolcanic character. The granodiorite was sampled at the locality Švihov and is composed of plagioclase, K-feldspar, quartz, biotite and amphibole.

The zircon population is uniformly yellow-brown, long-prismatic and euhedral, and three grains were evaporated individually, yielding identical $^{207}Pb/^{206}Pb$ ratios that combine to a mean age of 340.1 ± 1.1 Ma (table 3, fig. 13). This is consistent with ages from similar calc-alkaline granodiorites from the Central Bohemian Pluton (Holub and others, 1997) and also with ages for granodiorite sills dated in the

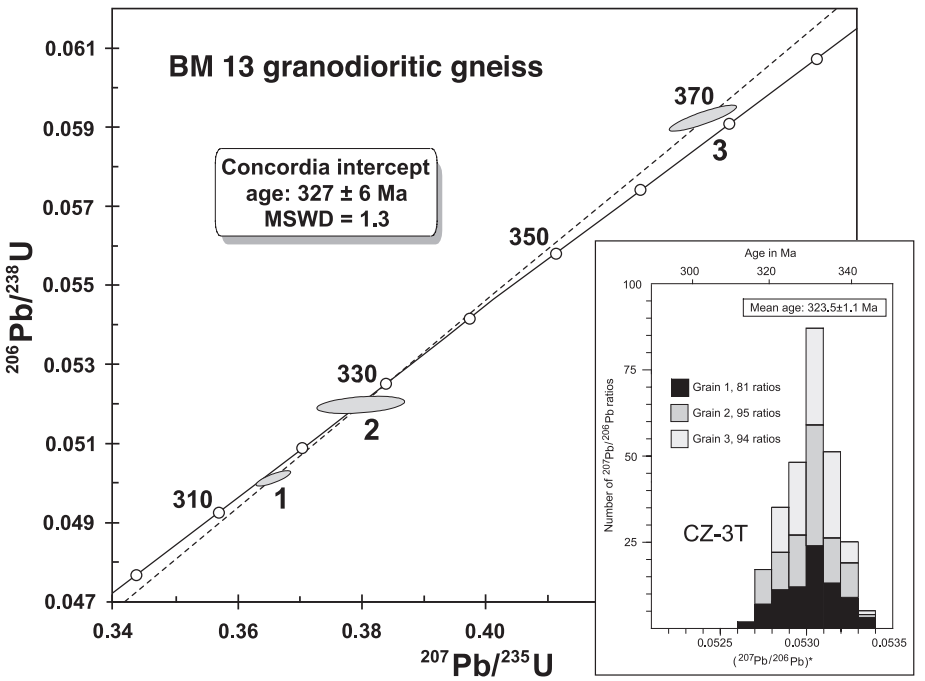

Fig. 12. Concordia diagram showing U-Pb zircon data for granodioritic gneiss sample BM 13. Inset is histogram showing distribution of radiogenic lead isotope ratios derived from evaporation of 3 zircon grains from granodiorite sample CZ/TAJ, integrated from 270 ratios.

northern part of the Bohemian Massif (Štípská and others, 2004). A common feature of all these granodioritic to tonalitic intrusions is their syntectonic, transpressional emplacement into upper crustal levels.

Pink granite sample BM 15 was collected at a dam on the Chrudimka River close to the village of Nasavrky (fig. 4). It is composed of K-feldspar, plagioclase, quartz and some biotite. Granophyric textures were observed locally. The granite caused contact metamorphism in the adjacent metasediments as indicated by the development of an orthitic chloritoid + muscovite + chlorite assemblage, indicating very low pressures and a shallow level of contact metamorphism. The Silurian country rocks exhibit evidence of intense compressional imbrication predating granite emplacement.

U-Pb dating results for abraded, originally subhedral, zircon fractions analyzed after vapor dissolution are presented in table 2 and in the Concordia diagram of figure 14. A fraction of pink, oval-shaped zircons and a fraction of two brown, sub-transparent grains are reversely discordant but plot close to concordia. They combine to an intercept age of 332 ± 20 Ma, whereas a third fraction containing 10 small, well rounded, abraded grains of originally clear euhedral shape produced a concordant $^{207}Pb/^{206}Pb$ age of 373 ± 25 Ma that may be interpreted to reflect an inherited component assimilated from wall rocks during ascent. However, since the fraction consisted of ten grains, the above "age" is most likely a geologically meaningless mixture between the 332 Ma populations and some older crustal component whose true age remains unspecified.

Resampling of the Nasavrky pink granite at the same locality as above (sample CZ/1Z) yielded clear, euhedral zircons, and evaporation of three grains produced a mean $^{207}Pb/^{206}Pb$ age of 332.2 ± 1.2 Ma (table 3, fig. 14, inset), identical to the

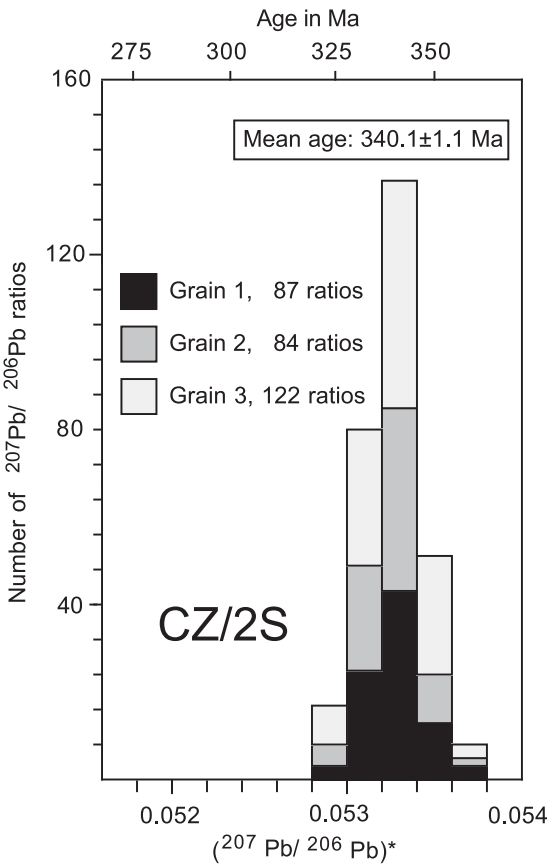

Fig. 13. Histogram showing distribution of radiogenic lead isotope ratios derived from evaporation of 3 zircon grains from granitoid gneiss sample CZ/2S, integrated from 320 ratios.

younger of the two vapor transfer results. No xenocrysts were identified in this sample. We are therefore confident, that the age of 332 reflects the time of emplacement of the pink granite.

Sm-Nd Whole-Rock Isotopic Systematics

Sm and Nd whole-rock isotopic data for most dated samples are listed in table 4 and are plotted in the isotopic evolution diagram of figure 15. Several samples show $^{147}Sm/^{144}Nd$ ratios considerably higher than 0.12 as is typically found in mature continental crust, and it is obvious that the light rare earth elements (LREE) in these samples have been modified by crystal fractionation involving LREE-enriched accessory phases such as apatite, or possibly metamorphism. Therefore, using these modified Sm/Nd ratios in the calculation of model ages yields meaningless data. However, it is helpful to use a 2-stage Nd isotopic evolution model (Liew and Hofmann, 1988) to calculate Nd mean crustal residence ages where the measured Sm/Nd ratio is used to define the isotopic evolution of the sample until its time of crystallization or its last modification of the Sm/Nd ratio (second stage), for example, metamorphism, migmatization or anatexis. The first (earlier) stage, namely the isotopic evolution path of Nd in the sample from its time of separation from the mantle, is then determined with an

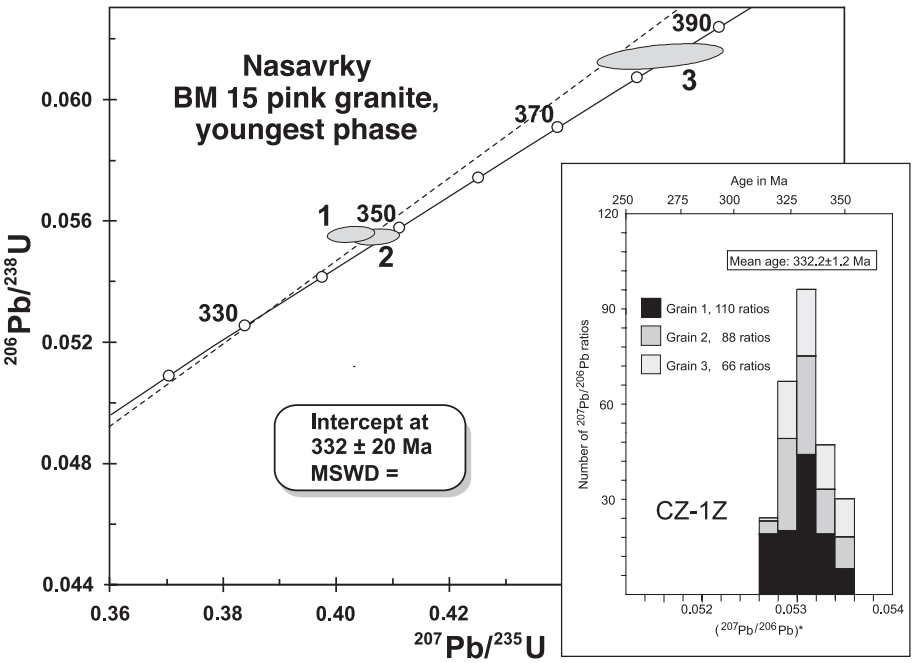

Fig. 14. Concordia diagram showing U-Pb zircon data for Zumberk pink granite-gneiss sample BM 15. Inset is histogram with distribution of radiogenic lead isotope ratios derived from evaporation of 3 zircons from pink granite-gneiss sample CZ/1Z, integrated from 264 ratios.

average crustal $^{147}Sm/^{144}Nd$ ratio of 0.12. The mean crustal residence ages thus calculated for the Bohemian granitoid rocks range from 1.43 to 1.96 Ga (fig. 15) and are considerably older than the magmatic protolith crystallization ages, indicating that substantial melting of older crustal sources must have occurred. The $\epsilon_{Nd(t)}$ values were calculated for the inferred times of high-grade metamorphism (340 Ma) or emplacement ages of the protoliths as determined by zircon dating.

As can be seen from figure 15, the majority of samples show $\epsilon_{Nd(t)}$ values of -3 to −8, consistent with melting of lower crustal material having an average mean crustal residence age of ~1.5 Ga. There is no evidence for involvement of significantly rejuvenated crust such as underplated, juvenile, mantle-derived material. Samples of ca. 400 to 500 Ma show similar $\epsilon_{Nd(t)}$ values, suggesting ongoing melting of isotopically similar crustal protoliths. Only during the latest Variscan development a "fanning-out" of the $\epsilon_{Nd(t)}$ values suggests involvement of limited amounts of juvenile material. When comparing the Bohemian root data with those from neighboring units, the data plot on the isotopic evolution paths of the gneisses from the Desná Dome and the Lugian Domain (Hegner and Kröner, 2000). This relationship suggests a uniform isotopic composition of different crustal levels in this part of the Bohemian Massif.

INTERPRETATION OF THE ISOTOPIC AGES

Isotopic Ages Testifying to Cambro-Ordovician Rifting along the Northern Gondwana Margin

The oldest rock of this study is represented by Gföhl Gneiss sample CZ 14/4 of the Internal Lower Crustal Belt with a protolith age of 550.6 ± 1.0 Ma (fig. 16). Similar or older Neoproterozoic ages are reported from the tectonic boundaries between the Varied and Monotonous Units of the Internal Middle Crustal Belt (for example,

TABLE 4

Sm-Nd isotopic data for samples from the Variscan root zone, southern Bohemia.

Sample	Sample	Age*	Nd [ppm]	Sm [ppm]	$^{147}Sm/^{144}Nd$	$^{143}Nd/^{144}Ndmeas.$	$^{143}Nd/^{144}Nd(t)$	e(t)	Model age [Ga]**
BM 1	Metarhyolite - Varied Group	350	11.21	2.33	0.1255	0.512104 ± 9	0.511817	-7.2	1.63
BM 2	Granitoid orthogneiss - Varied Group	350	4.22	1.47	0.1099	0.512204 ± 19	0.511952	-4.6	1.42
BM 3	Rhyolite - Drosendorf Group	530	5.78	1.70	0.1780	0.512072 ± 12	0.511454	-9.8	1.96
BM 4	Granitoid orthogneiss - Gföhl unit	400	8.98	2.41	0.1625	0.512195 ± 9	0.511769	-6.9	1.64
BM 5	Migmatite - Gföhl unit	350	15.37	3.74	0.1470	0.512199 ± 8	0.511862	-6.4	1.56
BM 6	Felsic granulite	390	9.03	2.33	0.1561	0.512193 ± 9	0.511794	-6.7	1.61
BM 7	Durbachite	320	58.6	12.66	0.1306	0.512119 ± 9	0.511846	-7.4	1.62
BM 8	Felsic granulite - Vir unit	350	4.09	1.02	0.1502	0.512252 ± 12	0.511907	-5.5	1.49
BM 9	Melt patch - Vir unit	310	9.75	1.95	0.1210	0.512521 ± 9	0.512275	0.7	0.97
BM10	Granite gneiss - Svratka complex	510	19.63	4.53	0.1394	0.512158 ± 9	0.511692	-5.7	1.63
BM11	Granite gneiss - Svratka complex	470	2.28	0.82	0.2161	0.512381 ± 11	0.511716	-6.2	1.64
BM12	Migmatite - Svratka complex	430	6.23	1.67	0.1616	0.512238 ± 8	0.511783	-5.9	1.58
BM13	Granodioritic gneiss	330	25.57	5.03	0.1190	0.512216 ± 9	0.511959	-5.0	1.43
BM14	Granodiorite - Nasavrky complex	350	3.88	0.49	0.1468	0.512284 ± 12	0.511948	-4.7	1.43
BM15	Pink biotite granite	330	28.98	5.40	0.1127	0.512279 ± 8	0.512036	-3.5	1.32

meas. = measured
*Crystallization age based on U-Pb or Pb-Pb zircon ages of this study.
**Nd model age, 2-stage Sm-Nd evolution after Liew and Hofmann (1988)

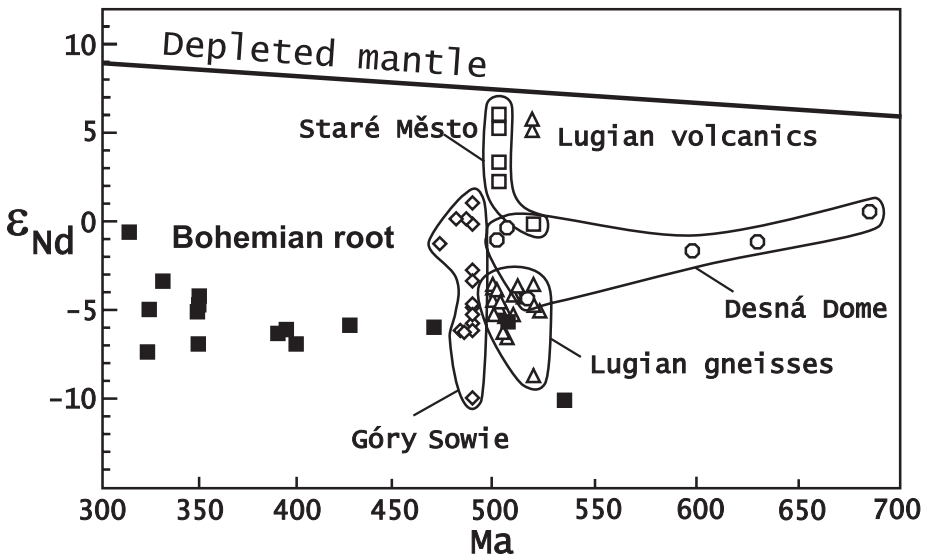

Fig. 15. Nd evolution diagram showing Sm-Nd systematics of dated samples of the Variscan root in southern Bohemia (full squares) compared with data for the Czech and Polish West Sudetes as compiled by Hegner and Kröner (2000).

Wendt and others, 1993; Gebauer and Friedl, 1994; Košler and others, 1996). These protolith ages show a striking similarity with those of adjacent Brunia granitoids (van Breemen and others, 1982; Scharbert and Batík, 1985; Fritz and others, 1996; Finger and others, 2000; Friedl and others, 2004) and granitoids of the Silesian Domain in the northerly West Sudetes (Kröner and others, 2000b).

Cambro-Ordovician magmatism is documented by zircon ages of samples BM 10 (515 ± 9 Ma) and BM 11, representing granitoid and volcanic rocks in the External Middle Crustal Belt (fig. 16). Both the zircon ages and Nd isotopic systematics of the studied Cambro-Ordovician gneisses from the EMC reveal remarkable similarities with calc-alkaline granitoid rocks in the West Sudetes which are interpreted to be of subduction-related origin (Kröner and others, 2000a, 2000b; Hegner and Kröner, 2000). Similar early Paleozoic emplacement ages of ~480 Ma for granitoid rocks have also been reported from the Gföhl gneiss in Lower Austria (Friedl and others, 1998, 2004) and from the Lower Crustal unit in South Bohemia (Vrána and Kröner, 1995). In addition, the onset of Ordovician-Silurian intracontinental rifting is documented by 428 ± 6 Ma old bimodal volcanism (Finger and von Quadt, 1995), now preserved in high-grade rocks of the Internal Lower Crustal Belt (Gföhl Unit in Lower Austria). Cambro-Ordovician volcanic activity was also reported from the upper crustal levels of the Teplá-Barrandian Unit (Chlupáč, 1994). However, the Brunia continent in general does not show such magmatism except in felsic dikes dated by Kröner and others (2000b) in the northern part of this segment (fig. 16). All these data are consistent with a concept of rifting along the northern Gondwana margin which, in the area of the Moldanubian domain, did not reach oceanic separation (Štípská and others, 2001). The intensity of Cambro-Ordovician deep crustal magmatic activity and volcanic and sedimentary additions at supracrustal levels are gradually increasing towards the northwest, leading to opening of the Saxothuringian ocean in between the Saxothuringian and Teplá-Barrandian domains (Franke, 2000). This Cambro-Ordovcian thinning of the Gondwana northern margin was recently interpreted either as a result of

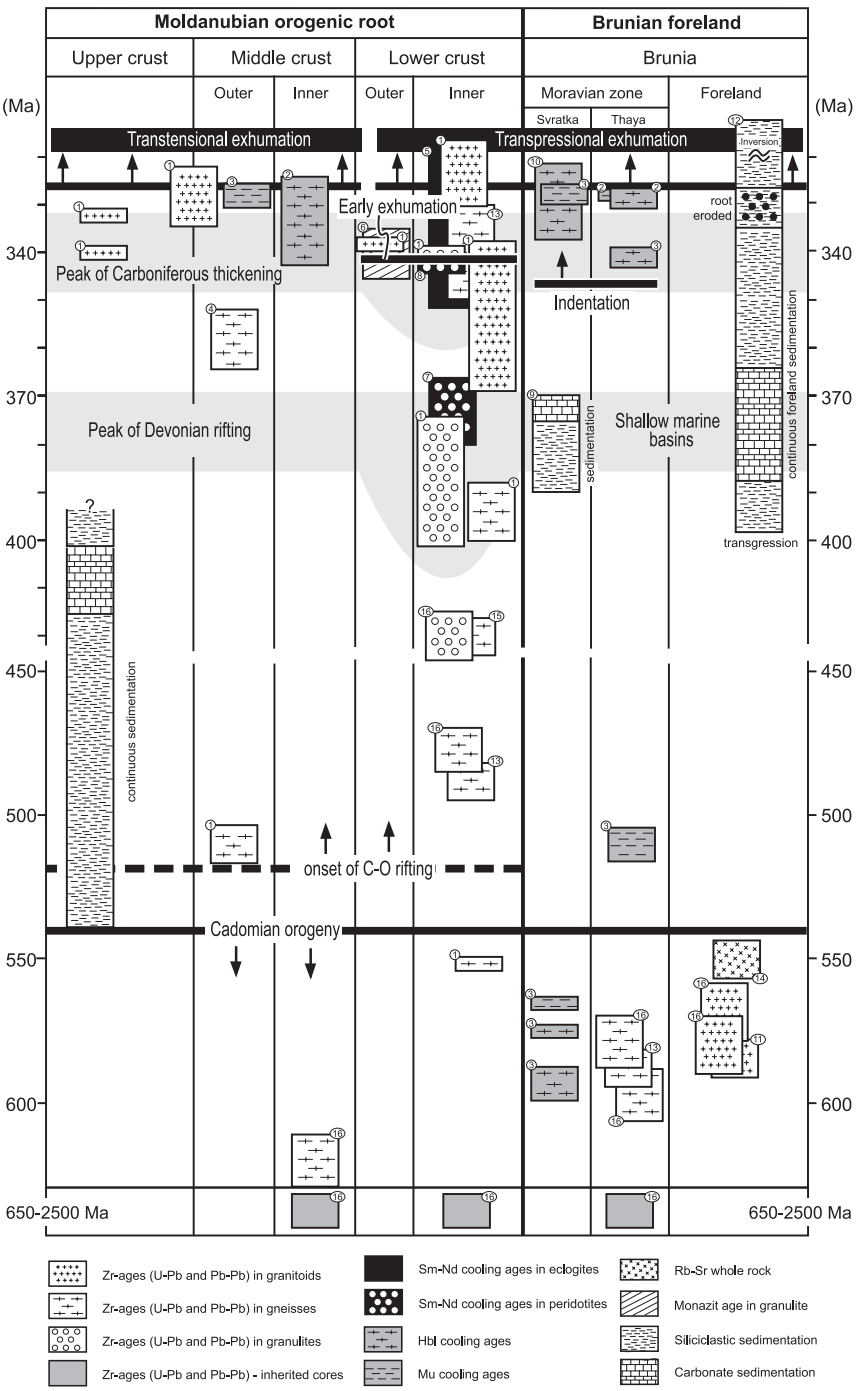

Fig. 16. Summary of published and new U-Pb and Pb-Pb zircon ages, published Nd-Sm cooling ages and published ^{40}Ar-^{39}Ar cooling ages from all crustal levels of the Moldanubian orogenic root and the Brunia continent from the entire eastern margin of the Bohemian massif (fig. 2). Stratigraphic columns of the Upper Crustal segment in the Barrandian area and the Brunia foreland according to Chlupáč (1994). Dark gray area in the diagram indicates duration of Paleozoic rifting as documented by geochronology and the sedimentary record. The light gray area shows the time span of compression including burial and

development of an intracontinental back arc basin above a giant subduction zone which must be located behind the Saxothuringian plate (Kröner and others, 2000b), or in terms of thinning of northern Gondwana (Winchester and others, 2002).

Isotopic Ages Testifying to Devonian Intracontinetal Back Arc Extension

A major change in plate configuration occurred in the early Devonian and was associated with subduction of the Saxothuringian Ocean to the southeast (in present-day coordinates; Franke, 1989; Krohe, 1998). This subduction led to the development of a magmatic arc in the region of Central Bohemian plutonic complex (Žák and others, 2005). During this period the Moldanubian domain occupied the position of a back-arc in the Saxothuringian subduction system (Carswell, 1991).

A Devonian age of 394 ± 6 Ma for zircons from Gföhl Gneiss samples BM 4 and 5 is interpreted to approximate the time of emplacement of the magmatic protoliths. Furthermore, we obtained an imprecise magmatic protolith age of 387 ± 14 Ma for felsic granulite sample BM 6 and 384.6 ± 1.1 for zircons in sample CZ-6 (fig. 16). U-Pb and Pb-Pb zircon protolith emplacement ages of 373 ± 12 Ma, 366.3 ± 1.1 Ma and 369 to 360 Ma were also reported from other Bohemian granulite massifs by Wendt and others (1994), Klemd and Bröcker (1999) and Štípská and others (2004), respectively. These ages agree well with a Devonian Sm-Nd cooling age of 373 Ma for nearby garnet peridotites from the ILC (Carswell and Jamtveit, 1990; Brueckner and others, 1991; table 1). Importantly, a late Devonian age of 358 Ma was also determined for felsic volcanic rocks of the IMC (Friedl and others, 1993), and massive magmatism represented by dolerite dykes occurred at the Silurian and Devonian boundary in the Paleozoic cover (Chlupáč, 1994).

A magmatic event leading to the emplacement of igneous rocks – precursors of felsic granulites, at 387 and 394 Ma, suggests a major period of magmatism in the Devonian. Our U-Pb and Pb-Pb data, combined with cooling ages for peridotites, may indicate an important Devonian thermal reworking of the Moldanubian lower crust. The products of volcanic activity preserved in the middle crustal Varied group support the existence of a Devonian basin that developed during crustal thinning (Finger and Steyrer, 1995). The timing of all these events correlates with first records of subduction activity at the eastern margin of the Saxothuringian domain (Franke, 2000) and with subsequent development of a magmatic arc in the area of the Central Bohemian Pluton (Košler and others, 1993; Holub and others, 1997; Venera and others, 2000). This concept is supported by geochemistry studies of garnet pyroxenite layers contained in garnet peridotites that indicate melting of sub-lithospheric mantle triggered by melts of fluids derived from subducting slab at greater depth (Becker, 1996a, 1996b). The geodynamic position of the Moldanubian domain with respect to the location of the subduction zone and related magmatic arc leads us to the conclusion, that the Devonian emplacement ages of magmatic rocks in the orogenic lower crust confirm the existence of a period of back arc extension in this region suggested by Carswell (1991).

A Devonian episode of shallow-water clastic sedimentation and volcanic activity was also reported from the western margin of Brunia (fig. 16). Here, deepening of the

---

exhumation of the lower crust related to the Brunia indentation process. The light gray area shows the duration of compression including burial and exhumation of the lower crust related to the Brunia indentation process. (1) – data of this study, (2) – Dallmeyer and others (1992), (3) – Fritz and others (1996), (4) – Friedl and others (1993), (5) – Brueckner and others (1991); Beard and others (1992), (6) – van Breemen and others (1982), (7) – Brueckner and others (1991), (8) - Beard and others (1992), (9) – Simplified after Galle and others (1995), (10) – Macintyre and others (1992), (11) – van Breemen and others (1982), (12) – Simplified after Kalvoda and others (2003) and Hartley and Otava (2001), (13) Friedl and others (1998), 14) – Scharbert and Batik (1985), (15) – Finger and von Quadt (1995), (16) – Friedl and others (2004).

Devonian sedimentary basin increased towards the north, where it was associated with voluminous bimodal volcanism and a deep marine sedimentary infill (Patočka and Valenta, 1990; Galle and others, 1995). This may indicate that the Brunia Neoproterozoic granitoids and metasediments represent a margin of the Devonian back arc domain, whereas the Monotonous Group corresponds to its highly stretched central part. We suggest that elevated temperatures during Devonian rifting may be responsible for significant melting of the lower part of the Neoproterozoic crust and crystallization of zircons from melts forming precursors of at least some varieties of the Gföhl gneiss and felsic granulites. In addition, numerical thermo-rheological models proposed by Thompson and others (2001) indicate that such a thermally weakened domain represents a suitable precursor for a thickened orogenic belt.

Isotopic Ages Related to Crustal Thickening

The youngest geochronological record pointing to a Devonian rifting process is represented by an U-Pb age of 358 Ma for felsic metavolcanic rocks reported by Friedl and others (1993) from the IMC (fig. 16). This age coincides remarkably well with termination of sedimentation within the early Paleozoic basin in the Prague area (fig. 1; Chlupáč, 1994). In addition, an angular unconformity between folded Givetian strata and overlying early Carboniferous sediments was reported from a drill hole reaching the base of the Cretaceous basin (in Chlupáč, 1994). The onset of convergence on the Brunia continent is marked by the transition from Famenian carbonate platform sedimentation to early Carboniferous flysh-type sediments at the Famenian-Frasnian boundary (Hartley and Otava, 2001). All these data indicate an important change in the tectonic regime at about 360 to 350 Ma (fig. 16).

The next younger reported ages correspond to the peak of high-pressure metamorphism in eclogites and granulites of the ILC and ELC. Metamorphic zircons from a HP granulite (sample CZ 6) yielded a $^{207}Pb/^{206}Pb$ evaporation age of 340.0 ± 1.1 Ma. A slightly older age of 353 ± 16 was obtained for magmatic emplacement of the Gföhl gneiss (samples BM4 and BM 5). This corresponds to ages from a nearby Ky-Kfs granulite (Kröner and others, 1988) and the Gföhl gneiss of the IMC, as well as an U-Pb monazite age for a granulite of the ILC (van Breemen and others, 1982). This age is also known from other granulite bodies elsewhere in the Bohemian Massif (Kotková and others, 1996; Kröner and Willner, 1998; Klemd and Bröcker, 1999; Kröner and others, 2000a; Svojtka and others, 2002; Štípská and others, 2004). Kröner and others (2000a) argued that the 340 Ma old zircons occur as inclusions in minerals defining the HP-phase as well as in the matrix and concluded that these zircons must have grown near or during peak pressure conditions.

The important discovery of this study is the age of syn-convergent calc-alkaline plutonism (340.1 ± 1.1 Ma; sample CZ/2S) for a granite intruding Paleozoic sediments in the upper crust (Hrouda and others, 1999). Corresponding ages of 350 to 340 Ma were reported for syn-convergent calc-alkaline plutons intruding upper crustal Paleozoic sediments (Holub and others, 1997; Janoušek and Gerdes, 2003) or thickened middle crustal units (Štípská and others, 2004). All these data suggest that the entire crust underwent progressive thickening during the early Carboniferous (fig. 16) after 10 to 20 Ma of convergence.

Relationship Between Isotopic Ages and the Exhumation Process

There are four important isotopic ages which permit to constrain the timing of exhumation processes related to the final structural pattern of the orogenic root. Mean ages of 341 ± 6 (sample BM 9) and 339.1 ± 1.1 Ma (sample CZ/Vir) were obtained from melt patches in high-temperature amphibolites associated with Ky-Kfs granulites of the ELC. The melting event is connected with retrogression of granulite and, therefore, reflects the earliest stage of the exhumation process. Similarily,

thrusting of the ILC over the IMC is dated by the emplacement of large portions of mantle-derived magmas of the Třebíč Massif dated at 340 Ma (Holub and others, 1997). This study yielded a group of ages from granitoids syntectonically emplaced along major intra-root tectonic boundaries and late granites intruding the upper crust. The age of durbachite emplacement (323 ± 7 and 323.5 ± 1.1 Ma; samples BM7 and CZ/TAJ) along the boundary between the ILC and EMC reflects the timing of oblique northeast-verging thrusting of the lower crust over the middle crust at a pressure of ~4 kbar (fig. 16). Similarly, the age of a syntectonic granodiorite (327 ± 6 and 323.5 ± 1.1 Ma; samples BM13 and CZ/3T) at the boundary between the EMC and UC suggests extensional unroofing along the middle/upper crustal boundary (Pitra and others, 1994). A similar age has been obtained for the youngest granite generation (332 ± 20 and 332.2 ± 1.1 Ma; samples BM15 and CZ/1Z) that intruded the previously folded upper crustal rocks along a major normal shear zone.

Our data are in agreement with emplacement ages for a large S-type granite pluton in the axial part of the IMC (see Finger and others, 1997 for review). The existing PT estimates for the contact aureole indicate a depth of emplacement corresponding to ~4 kbar (Petrakakis, 1997). The above-listed ages correspond to numerous muscovite and biotite Ar-Ar data from the EMC, ELC and metamorphosed Brunia-derived nappes from the eastern margin of the Bohemian Massif ranging between 330 and 325 Ma (Dallmeyer and others, 1992; Fritz and others, 1996). The $^{40}Ar/^{39}Ar$ ages from the internal part of the root reflect a similar time span (Dallmeyer and others, 1992). A-type eclogites from our study area yielded Sm-Nd cooling ages of 336 ± 16 and 323 ± 7 Ma respectively, which have been interpreted as exhumation ages (Beard and others, 1992). However, other Sm-Nd data reported from root eclogites suggest older cooling ages up to 377 Ma (Brueckner and others, 1991; Beard and others, 1992; Klemd and Bröcker, 1999). The tectonic setting of the eclogites is often poorly constrained and, therefore, these cooling ages are difficult to interpret.

A study of heavy minerals from sediments in the foreland basin documented the first appearance of a garnet-rich heavy mineral assemblage at the beginning of the late Visean (~335 Ma), indicating the first exhumation of high-grade metamorphic rocks (Hartley and Otava, 2001). The most important evidence for exhumation of the orogenic lower crustal rocks is the presence of granulite-facies rocks, durbachites and migmatites in pebbles within middle Visean conglomerates, indicating the onset of deposition of lower crustal material in the foreland basin at around 330 to 327 Ma (Hartley and Otava, 2001). These granulitic pebbles experienced their high-pressure metamorphism at ~340 Ma (Vrána and Novák, 2000; Kotková and others, 2001). All the above data indicate that exhumation of rocks from the bottom of the root to the surface occurred within a time span of 10 to 15 Ma (fig. 16). Such a high exhumation rate has already been estimated by Svojtka and others (2002) and Štípská and others (2004) for other parts of the Bohemian Massif.

GEODYNAMIC INTERPRETATION

The rapid transition from Devonian rifting to shortening at about 350 Ma ago (fig. 17B) indicates that the entire lithosphere in the domain of the future orogenic root was exceptionally weak, because there was a very short period of temperature decay before the onset of collision (Loosveld and Etheridge, 1990). As shown by Thompson and others (2001) and Schulmann and others (2002) such a weakened lithosphere can be homogeneously thickened. Their calculations show that a thickening timescale of 10 to 15 Ma is required to transport the Moho to a depth of 60 km without significant heat transfer. Therefore, temperatures of 800 to 900 °C recorded at peak pressures of 18 to 20 kbar in eclogites and HP granulites (Steltenpohl and others, 1993; Medaris and others, 1998), may correspond to temperatures existing in the lower crust of the rifted domain prior to thickening (Štípská and Powell, 2005a, 2005b). We assume that

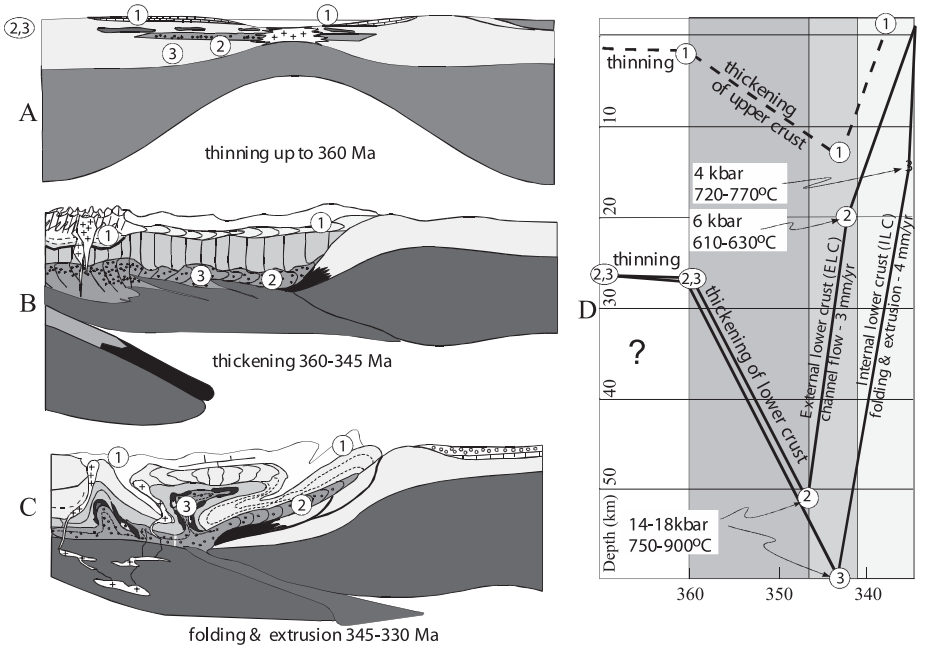

Fig. 17. Series of evolutionary cross sections through the eastern margin of the Variscan orogen showing: (A) Development of large-scale intracontinental rifting during the Devonian between 390 and 360 Ma. (B) Geometry of root units at ~350 Ma prior to exhumation along eastern margin of Bohemian Massif. (C) Geometry of root and continental margin during exhumation at ~340 Ma associated with channel flow of lower crust along the external part of the root and folding of the entire crustal sequence in the more internal part of the root. (D) Depth-time diagram showing integrated rates of thickening following lithospheric thinning and subsequent exhumation, relative to several P-T constraints from geothermobarometry (Medaris and others, 1995a; Schulmann and others, 1999; Tajcmanova and others, 2005). Two lines are constructed for exhumation along a lower crustal antiform and orogenic channel, respectively, on the assumption of a lower pressure for granulite-facies metamorphism in the EMC and higher pressure in the ILC, respectively.

the thickening process led to the formation of a root composed of three horizontal crustal layers defined by maximum pressure conditions estimated for individual lithologies of thickened lower crust (18 – 20 kbar), middle crust (8 – 10 kbar) and upper crust (4 kbar), respectively (fig. 17B). The tectonic model presented here can be compared with modern thermomechanical models in which the mechanical and metamorphic evolution of large convergent orogens is driven by subduction of suborogenic mantle lithosphere (Willet and others, 1993; Beaumont and others, 2004). Evolution of continental plateaus above subducting mantle lithosphere was modeled by Vanderhaeghe and others (2003) as a result of prolonged thickening of the crust during orogenesis. However, this model of crustal thickening is connected with long lasting growth of a plateau 750 km wide during ~75 Ma and is not associated with a pre-existing thermal anomaly.

Indentation-Induced Lower Crustal Flow and Exhumation

Our model of exhumation of lower crust in the study area is based on the assumption that after thickening the buried sub-rift (sub-root) upper mantle becomes stronger than the adjacent continental mantle below a depth of 60 to 70 km. We assume that any further descent of the root is blocked, but the lower crust in the thickened domain is significantly weaker than the adjacent continental mantle.

Consequently, the Moldanubian sub-root mantle was underthrust below the Brunia continental mantle at about 350 to 340 Ma (figs. 17 B, C). This led to continuous convergent motion of the Brunia indenter in form of a lithospheric flake, and the Brunia upper mantle slid along the sub-root rigid floor of the mantle wedge and squeezed the weak parts of the inner root upwards. It is this indentation process that generated major shortening of the root domain, leading to perturbation of its original horizontal rheological stratification. In our view, the exhumation of deeply buried crust is the result of a continuous indentation process of the Brunia continent in front of which granulitized lower crust was rapidly extruded to higher crustal levels. We suggest that the alternation of crustal levels presented in this study resulted from folding of these horizontal rheological boundaries in form of a large lower crustal antiform in front of the indenting plate. The laterally different extent of vertical amplification of the lower crustal antiform representing the future ILC belt was controlled by the thickness of the indenting Brunia ramp.

The mechanism of initiation of the original cusp at the lower-middle crustal boundary, the amplification of folds, and final transition to flat fabrics into mid-crustal levels by a lateral spreading mechanism is explained and discussed elsewhere (Štípská and others, 2004). Here we only discuss the finite geometry of the root crustal level by combined mechanisms of folding of the lower and middle crustal interface and ductile extrusion of the lower crust close to the indenting continental lithosphere. The lower crustal rocks were also extruded along a narrow zone or channel following the boundary of the Brunia indenter forming the ELC belt. The extrusion of weak lower crustal material led to a high ascent velocity of HP rocks to a shallow crustal level as shown by the steep decompression PT path for eclogites (Konopásek and others, 2002). A high exhumation velocity is documented by the 338 ± 3 Ma monazite U-Pb age from fresh granulite (van Breemen and others, 1982), 340 Ma U-Pb zircon age for a melt patch in opx-bearing amphibolite surrounding a granulite body (Sample BM 9, this work), and a ^{40}Ar-^{39}Ar amphibole cooling age of 340 Ma in nearby retrograde eclogites at the Brunia margin (Macintyre and others, 1992). Since the ages of the low pressure overprint and peak conditions of granulite metamorphism (Schulmann and others, 1999) are identical, within analytical error, we must consider the time span indicated by the error in the least precise age, which is a maximum of 6 Ma. Therefore, the extrusion rate within the ELC belt corresponds to ~7 mm/y (fig. 17C). This indicates that the lower crustal rocks reached shallow crustal levels earlier in the area of the ELC belt than in the lower crustal antiform farther to the west. Moreover, the rate of vertical extrusion in this belt is significantly higher compared to calculated exhumation rates of granulites in the large-scale antiform of the ILC belt estimated at about 3 mm/y (Tajčmanová and others, 2005).

Comparison of orogenic structure of eastern margin of the Bohemian Massif with existing numerical models shows the development of a lower crustal antiform and asymmetrical upper crustal thickening similar to results shown by Jamieson and others (2002). However, their latest models show the effects of doming triggered by underthrusting of rigid lower crust, extrusion of the dome in a channel above the frontal ramp or near-symmetric thrust extrusion located on the side of the orogen adjacent to subducting plate (Beaumont and others, 2004, fig. 12), which is in contradiction with distribution of lower crustal rocks along the eastern margin of the Bohemian Massif.

Late Transpressional and Transtensional Deformation

The most prominent late tectonic feature in the Carboniferous evolution of the eastern margin of the Bohemian Massif is dextral transpressive deformation along the Brunia margin (Schulmann, 1990; Fritz and Neubauer, 1993; Schulmann and others, 1994). This deformation was connected with large-scale oblique folding of Brunia-derived crystalline nappes (Štípská and others, 2000). The age of these processes is well

constrained at 325 to 300 Ma by ^{40}Ar-^{39}Ar ages (Fritz and others, 1996). The durbachite bodies dated at 323 Ma in this study and emplaced along the ILC and EMC boundary, display a magmatic to solid-state fabric consistent with dextral shearing. Reactivation of these major tectonic boundaries indicates that the horizontal shear stress was also transmitted into the root.

The other important feature of the northern part of the study area is the continuous change of fabric orientation towards parallelism with the Elbe shear zone. Here, transpressive NE-SW trending deformation parallel to the Brunia margin progressively passes into transtensional dextral shearing and extensional deformation in a region parallel to the Elbe zone (Melka and others, 1992; Pitra and others, 1994). The age of this shearing is well constrained by syn-extensional emplacement of a granodiorite sill along the EMC-UC boundary and by dating of emplacement of an S-type granite in the upper crust that is also coeval with NW-directed normal shearing. These deformations were responsible for exhumation of middle crust up to 4 kbar in conjunction with downthrow of the upper crust to similar depth (Pitra and Guiraud, 1996). Hence, our study has shown that dextral transpressive shearing parallel to the root-continent boundary, and dextral transtension parallel to the Elbe zone operated at the same time and at similar crustal levels. This deformation was restricted to a maximum distance of 20 km from the continental margin and the Elbe zone, but had a profound effect on the final geometrical pattern of the study area. Transpressive shearing along Brunia and transtensional deformation parallel to the Elbe zone were responsible for displacement of the ELC and EMC to the northeast and their dramatic attenuation in the south. The upper crustal segment, which was originally sitting upon the EMC, was extended, thinned and transported to the NW along a major normal shear zone. If the combined effect of NE-directed transpression and NW-transtension is removed, a simple tectonic pattern emerges, resulting from the early stages of large-scale buckling and an orogenic channel parallel to the Brunia margin. This pattern is manifested by alternating belts of lower and middle crust parallel to the main collisional boundary.

In order to explain simultaneous compression and transtension along the root margins, a tectonic model implying far-field forces is proposed. Edel and others (2003) suggested that the Carboniferous evolution of the Variscan belt can be regarded as the result of major clockwise rotation of a previously assembled orogenic system, compensated by large, dextral NW-SE striking lithospheric faults (fig. 5 in Edel and others, 2003). The blocks defined by these faults are antithetically rotating in a book-shelf manner and thus produced anticlockwise rotations. We suggest that the dextral shearing parallel to the Elbe zone is fully compatible with the model proposed by Edel and others (2003), but its activity must have been accompanied by clockwise rotation of the Brunia block, producing coeval transpressive deformation of the eastern margin of the root. These authors suggested that rotation of the Variscan belt was most likely initiated by closure of the westerly located Rhenohercynian ocean during the early Carboniferous (Oncken and others, 1999; Franke, 2000) which correlates well with the above-described transpressive and transtensional movements during the time span of 330 to 320 Ma.

ACKNOWLEDGMENTS

This research resulted from a collaborative project between Charles University, Prague, and Mainz and Munich Universities, Germany. Financial support to Karel Schulmann by the Czech Science Foundation (grant no. 2005/98/K004) is gratefully acknowledged. The isotopic work was funded by the German Science Foundation (DFG, grant Kr 68-1) to Alfred Kröner and Ernest Hegner. Karel Schulmann, Ondrej Lexa, Pavla Štípská, and Jiří Konopásek also received financial support from the Czech Ministry of Education, grant no. 24313005, Alfred Kröner acknowledges the use of

mass spectrometer analytical facilities in the Max-Planck-Institut für Chemie in Mainz. Thorough reviews of Onno Oncken, Patrick O'Brien, Jean Pierre Burg and John Dewey significantly helped to improve the manuscript and are gratefully acknowledged.

Appendix: analytical procedures

Zircons were separated using a Wilfley table, magnetic separator, heavy liquids, and final handpicking under a binocular microscope. In order to obtain information on the internal structures and zircon morphologies, cathodoluminiscence (CL) and back scatter electron (BSE) images were studied before selecting zircons for isotopic analysis.

U-Pb Zircon Analysis after Vapor Transfer

Single zircon grains or small grain fractions consisting of morphologically identical grains were dissolved by the vapor transfer technique (Krogh, 1978; Parrish, 1987; Wendt and Todt, 1991). The method requires no chemical separation of U and Pb and produces low degrees of sample contamination (typically ~3 pg Pb blank contribution per zircon sample). For blank corrections the following Pb ratios were used: $^{206}Pb/^{204}Pb = 18.15$; $^{207}Pb/^{204}Pb = 15.63$; $^{208}Pb/^{204}Pb = 38.14$. As samples were not weighed prior to decomposition, U and Pb concentrations could not be determined. However, use of a mixed $^{205}Pb/^{233}U$ spike solution enabled us to calculate the the U/Pb ratios and corresponding U-Pb ages.

Isotopic ratios were measured on a Finnigan-MAT 261 mass spectrometer equipped with a secondary electron multiplier at the University of Munich. The analytical data and calculated ages are listed in table 2 and were corrected for instrumental mass fractionation (ca. 2. 2 ‰ per atomic mass unit) and total procedural blank (<10 pg Pb per analysis). Regression analysis of the U-Pb isotopic data was performed with the ISOPLOT program of Ludwig (1999), using the algorithm of York (1969) and the decay constants recommended by Steiger and Jäger (1977). Errors are at the 2-sigma (95% confidence) level.

Zircon Evaporation

Single zircons or small grain fractions of 3 to 4 crystals each were handpicked after careful optical inspection and analyzed by the evaporation method (Kober, 1987). $^{207}Pb/^{206}Pb$ isotopic ratios were measured on a Finnigan-MAT 261 mass spectrometer at the Max-Planck-Institut für Chemie in Mainz. The procedures as well as comparisons with conventional and ion-microprobe zircon dating are detailed in Kröner and others (1991) and Kröner and Hegner (1998).

The calculated ages and their uncertainties are based on the means of all ratios and their 2-σ (mean) errors. Mean ages and errors for several zircons from the same sample are presented as weighted means of the entire data set. Repeated analysis of an internal zircon standard suggests an error of about 0.2 percent as best estimate for the reproducibility of the $^{207}Pb/^{206}Pb$ ages. In the case of combined data sets the 2-σ_m error may become very low, and whenever this error was less than the reproducibility of the internal standard, we have used the latter value (that is, 0.2 %).

The zircon evaporation data are presented in table 3, and the $^{207}Pb/^{206}Pb$ spectra are shown in histograms that permit visual assessment of the data distribution. Due to the lack of U concentrations there is no *a priori* way to determine whether the zircons behaved as closed systems and the measured $^{207}Pb/^{206}Pb$ ratio reflects a concordant age. However, comparative studies using evaporation, conventional U–Pb dating, and ion-microprobe analysis have shown excellent agreement, even for zircons from complex metamorphic terrains (Kröner and others, 1991, 2001; Cocherie and others, 1992; Jaeckel and others, 1997; Karabinos, 1997).

Sm-Nd Whole-Rock Isotopic Analysis

Sm and Nd isotopes of whole-rock samples were analyzed at the University of Munich, employing procedures outlined in Hegner and others (1995). The Nd isotopic ratios were measured in a dynamic quadruple mass collection mode using a Finnigan MAT 261, whereas a static collection mode was used for Sm isotopes. $^{143}N/^{144}Nd$ isotope ratios were normalized to $^{146}Nd/^{144}Nd \cong 0.7219$ and Sm isotopic ratios to $^{147}Sm/^{152}Sm = 0.56081$. Total procedural blanks were ca. 70 pg Nd and ca. 20 pg Sm. Within-run precision ($2\sigma_{mean}$) for $^{143}Nd/^{144}Nd$ was $\pm$ 1.3 x 10^{-5}. Repeated measurements of the $^{143}N/^{144}Nd$ isotopic ratio in our Ames Nd standard yielded a value of 0.512138 $\pm$ 12 (2σ, N= 26), corresponding to 0.511850 in the La Jolla Nd standard. The Nd model ages were calculated with a 2-stage isotopic evolution model as defined in Liew and Hofmann (1988) due to the fact that about half of the samples have high Sm/Nd ratios, unlike typical continental crust, thus preventing the calculation of meaningful single-stage Nd model ages as outlined in

DePaolo (1981). The Sm-Nd isotopic data and Nd model ages are listed in table 4. We interpret the Nd model ages in terms of mean crustal residence ages (Arndt and Goldstein, 1987).

References

Arndt, N. T., and Goldstein, S. L., 1987, Use and abuse of crust-formation ages: Geology, v. 15, p. 893–895.

Beard, B. L., Medaris, L. G., Johnson, C. M., Brueckner, H. K., and Mísař, Z., 1992, Petrogenesis of Variscan high-temperature group-A eclogites from the Moldanubian zone of the Bohemian Massif, Czechoslovakia: Contributions to Mineralogy and Petrology, v. 111, p. 468–483.

Beaumont, C., Jamieson, R. A., Nguyen, M. H., and Medvedev, S., 2004, Crustal channel flows: 1. Numerical models with applications to the tectonics of the Himalayan-Tibetan orogen: Journal of Geophysical Research, v. 109, B06406.

Becker, H., 1996a, Crustal trace element and isotopic signatures in garnet pyroxenites from garnet peridotites massifs from lower Austria: Journal of Petrology, v. 37, p. 785–810.

——— 1996b, Geochemistry of garnet peridotite massifs from lower Austria and the composition of deep lithosphere beneath a Paleozoic convergent plate margin: Chemical Geology, v. 134, p. 49–65.

Brueckner, H. K., Medaris, L. G., and Bakun-Czubarow, N., 1991, Nd-Sm age and isotope patterns from Variscan eclogites of the eastern Bohemian Massif: Neues Jahrbuch für Mineralogie-Abhandlungen, v. 163, p. 169–196.

Carswell, D. A., 1991, Variscan high P-T metamorphism and uplift history in the Moldanubian Zone of the Bohemian Massif in Lower Austria: European Journal of Mineralogy, v. 3, p. 323 – 342.

Carswell, D. A., and Jamtveit, B., 1990, Variscan Sm-Nd ages for the high-pressure metamorphism in the Moldanubian Zone of the Bohemian Massif, Lower Austria: Neues Jahrbuch für Mineralogie-Abhandlungen, v. 162, p. 69–78.

Chlupáč, I., 1994, Facies and biogeographic relationships in Devonian of the Bohemia Massif: Courier Forschungsintitut Senckenberg, v. 169, p. 299–317.

Cocherie, A., Guerrot, C., and Rossi, P., 1992, Single-zircon dating by step-wise Pb evaporation – comparison with other geochronological techniques applied to the Hercynian granites of Corsica, France: Chemical Geology, v. 101, p. 131–141.

Dallmeyer, R. D., Neubauer, F., and Höck, V., 1992, Chronology of Late Paleozoic tectonothermal activity in the southeastern Bohemian Massif, Austria (Moldanubian and Moravo-Silesian zones) - Ar^{40}/Ar^{39} mineral age controls: Tectonophysics, v. 210, p. 135–153.

DePaolo, D. J., 1981, A Nd and Sr isotopic study of Mesozoic calc-alkaline granitic batholiths of the Sierra Nevada and Peninsular Ranges, California: Journal of Geophysical Research, v. 86, p. 10370–10488.

Dewey, J. F., and Bird, J. M., 1970, Mountain belts and the new global tectonics: Journal of Geophysical Research, v. 75, p. 2625–2647.

Dewey, J. F., and Burke, K., 1973, Tibetan, Variscan and Precambrian basement reactivation: Products of continental collision: Journal of Geology, v. 81, p. 683–692.

Dudek, A., 1980, The crystalline basement block of the Outer Carpathians in Moravia: Rozpravy Československé Akademie Věd, v. 90, p. 1–85.

Dudek, A., and Fediuková, E., 1974, Eclogites of the Bohemian Moldanubicum: Neues Jahrbbuch für Mineralogie Abhandlungen, v. 121, p. 127–159.

Edel, J. B., Schulmann, K., and Holub, F. V., 2003, Anticlockwise and clockwise rotations of the Eastern Variscides accommodated by dextral lithospheric wrenching: palaeomagnetic and structural evidence: London, Journal of the Geological Society, v. 160, p. 209–218.

Finger, F., and Steyrer, H. P., 1995, A tectonic model for the eastern Variscides: Indications from a chemical study of amphibolites in the south-eastern Bohemian Massif: Geologica Carpatica, v. 46, p. 137–150.

Finger, F., and von Quadt, A., 1995, U/Pb ages of zircons from a plagiogranite-gneiss in the SE Bohemian Massif, Austria – further evidence for an important early Palaeozoic rifting episode in the eastern Variscides: Schweizerische Mineralogische und Petrographische Mitteilungen, v. 75, p. 265–270.

Finger, F., Roberts, M. P., Haunschmid, B., Schermaier, A., and Steyrer, H. P., 1997, Variscan granitoids of central Europe: their typology, potential sources and tectonothermal relations: Mineralogy and Petrology, v. 61, p. 67–96.

Finger, F., Tichomirowa, M., Pin, C., and Hanžl, P., 2000, Relics of an early-Panafrican metabasite-metarhyolite formation in the Brno Massif, Moravia, Czech Republic: International Journal of Earth Sciences, v. 89, p. 328–335.

Franců, E., Franců, J., Kalvoda, J., Poelchau, H. S., and Otava, J., 2002, Burial and uplift history of the Palaeozoic Flysch in the Variscan foreland basin (SE Bohemian Massif, Czech Republic), *in* Bertotti, G., Schulmann, K., and Cloetingh, S., editors, Continental collision and the tectonosedimentary evolution of forelands: European Geophysical Society, Stephen Mueller Special Publication Series, v. 1, p. 167–179.

Franke, W., 1989, Variscan plate tectonics in Central Europe – current ideas and open questions: Tectonophysics, v. 169, p. 221–228.

——— 2000, The mid-European segment of the Variscides: tectonostigratigraphic units, terrane boundaries and plate tectonic evolution, *in* Franke, W., Haak, W., Oncken, O., and Tanner, D., editors, Orogenic processes: Quatification and modelling in the Variscan belt: Geological Society of London Special Publication, v. 179, p. 35–63.

Friedl, G., von Quadt, A., Ochsner, A., and Finger, F., 1993, Timing of the Variscan orogeny in the Southern Bohemian Massif (NE Austria) deduced from new U-Pb zircon and monazite dating: Terra Abstracts, v. 5, p. 235–236.

Friedl, G., McNaughton, N., Fletcher, I. R., and Finger, F., 1998, New SHRIMP-zircon ages for orthogneisses from the south-eastern part of the Bohemian Massif (Lower Austria), *in* Schulmann, K., editor, Proceedings of the International conference - Palaeozoic orogenesis and crustal evolution of European lithosphere: Acta Universitatis Carolinae, v. 42, p. 251–252.

Friedl, G., Finger, F., Paquette, J. L., von Quadt, A., McNaughton, N. J., and Fletcher, I. R., 2004, Pre-Variscan geological events in the Austrian part of the Bohemian Massif deduced from U-Pb zircon ages: International Journal of Earth Sciences, v. 93, p. 802–823.

Fritz, H., and Neubauer, F., 1993, Kinematics of crustal stacking and dispersion in the south-eastern Bohemian massif: Geologische Rundschau, v. 82, p. 556–556.

Fritz, H., Dallmeyer, R. D., and Neubauer, F., 1996, Thick-skinned versus thin-skinned thrusting: rheology-controlled thrust propagation in the Variscan collisional belt (the southeastern Bohemian Massif, Czech Republik - Austria): Tectonics, v. 15, p. 1389–1413.

Fuchs, G., 1986, Zur Diskussion um den Deckenbau der Böhmischen Masse: Jahrbuch der Geologischen Bundesanstalt, v. 129, p. 41–49.

Fuchs, G., and Matura, A., 1976, Die Geologie des Kristallins der südlichen Böhmischen Masse: Jahrbuch der Geologischen Bundesanstalt, v. 119, p. 1–43.

Galle, A., Hladil, J., and Isaacson, P. E., 1995, Middle Devonian biogeography of closing south Laurussia – North Gondwana Variscides: Examples from the Bohemian Massif (Czech Republic), with emphasis on Horní Benešov: Palaios, v. 10, p. 221–239.

Gebauer, D., and Friedl, G., 1994, A 1.38 Ga protolith age for the Dobra orthogneiss (Moldanubian Zone) of the southern Bohemian Massif, NE-Austria); evidence from ion-microprobe (SHRIMP) dating of zircon: Journal of the Czech Geological Society, v. 39, p. 34–35.

Hartley, A. J., and Otava, J., 2001, Sediment provenance and dispersal in a deep marine foreland basin: the Lower Carboniferous Culm Basin, Czech Republic: Journal of the Geological Society London, v. 158, p. 137–150.

Hegner, E., and Kröner, A., 2000, Review of Nd isotopic data and xenocryst and detrital zircon ages from the pre-Variscan basement in the eastern Bohemian Massif: speculations on palinspasic reconstructions, *in* Franke, W., Haak, V., Oncken, O., and Tanner, D., editors, Orogenic processes: quantification and modelling in the Variscan belt: Geological Society of London Special Publication, no. 179, p. 113–129.

Hegner, E., Walter, H. J., and Satir, M., 1995, Pb-Sr-Nd isotopic compositions and trace element geochemistry of megacrysts and melilitites from the Tertiary Urach volcanic field: source composition of small volume melts under SW Germany: Contributions to Mineralogy and Petrology, v. 122, p. 322–335.

Holub, F. V., Cocherie, A., and Rossi, P., 1997, Radiometric dating of granitic rocks from the Central Bohemian Plutonic Complex (Czech Republic); constraints on geochronology of thermal and tectonic events along the Moldanubian-Barrandian boundary: Comptes Rendus de 'l Academie des Sciences, Serie II, v. 325, p. 19–26.

Hrouda, F., Táborská, Š., Schulmann, K., Ježek, J., and Dolejš, D., 1999, Magnetic fabric and rheology of co-mingled magmas in the Nasavrky Plutonic Complex (E. Bohemia): implications for intrusive strain regime and emplacement mechanism: Tectonophysics, v. 307, p. 93–111.

Jaeckel, P., Kröner, A., Kamo, S. L., Brandl, G., and Wendt, J. I., 1997, Late Archaean to early Proterozoic granitoid magmatism and high-grade metamorphism in the central Limpopo belt, South Africa: London, Journal of the Geological Society, v. 154, p. 25–44.

Jamieson, R. A., Beaumont, C., Nguyen, M. H., and Lee, B., 2002, Interactions of metamorphism, deformation and exhumation in large convergent orogens: Journal of Metamorphic Geology, v. 20, p. 9–24.

Janoušek, V., and Gerdes, A., 2003, Timing the magmatic activity within the Central Bohemian Pluton, Czech Republic: Conventional U-Pb ages for the Sázava and Tábor intrusions and their geotectonic significance: Journal of the Czech Geological Society, v. 48, p. 70–71.

Kalvoda, J., Leichmann, J., Bábek, O., and Melichar, R., 2003, Brunovistulian Terrane (Central Europe) and Istanbul Zone (NW Turkey): Late Proterozoic and Paleozoic tectonostratigraphic development and paleogeography: Geologica Carpathica, v. 54, p. 139–152.

Karabinos, P., 1997, An evaluation of the single-grain zircon evaporation method in highly discordant samples: Geochimica et Cosmochimica Acta, v. 61, p. 2467–2474.

Klemd, R., and Bröcker, M., 1999, Fluid influence on mineral reactions in ultrahigh-pressure granulites: a case study in the Snieznik Mts. (West Sudetes, Poland): Contributions to Mineralogy and Petrology, v. 136, p. 358–373.

Kober, B., 1987, Single-zircon evaporation combined with Pb+emitter-bedding for $^{207}Pb/^{206}Pb$-age investigations using thermal ion mass spectrometry, and implications to zirconology: Contributions to Mineralogy and Petrology, v. 96, p. 63–71.

Kolenovská, E., Schulmann, K., Klápová, H., and Štípská, P., 1999, Tectonometamorphic evolution of the Moldanubian zone near Jemnice (south Moravia, Bohemian Massif): Beihefte zur European Journal of Mineralogy, v. 11, p. 91–110.

Konopásek, J., Schulmann, K., and Johan, V., 2002, Eclogite-facies metamorphism at the eastern margin of the Bohemian Massif - subduction prior to continental underthrusting?: European Journal of Mineralogy, v. 14, p. 701–713.

Košler, J., Aftalion, M., and Bowes, D. R., 1993, Mid-Late Devonian plutonic activity in the Bohemian Massif - U-Pb zircon isotopic evidence from the Staré Sedlo and Mirotice gneiss complexes, Czech Republic: Neues Jahrbuch für Mineralogie – Monatshefte, v. 9, p. 417–431.

Košler, J., Aftalion, M., Vokurka, K., Klečka, M., and Svojtka, M., 1996, Early Cambrian granitoid magmatism in the Moldanubian Zone: U-Pb zircon isotopic evidence from the Stráž orthogneiss (in Czech): Zprávy o geologických výzkumech - ČGU Praha, p. 109–110.

Kotková, J., Kröner, A., Todt, W., and Fiala, J., 1996, Zircon dating of north Bohemian granulites, Czech Republic: Further evidence for the lower carboniferous high-pressure event in the Bohemian Massif: Geologische Rundschau, v. 85, p. 154–161.

Kotková, J., Novák, M., Leichmann, J., and Houzar, S., 2001, Nature and Provenance of Exotic Rock Types from Lower Carboniferous Conglomerates (Eastern Bohemian Massif): Geolines, v. 13, p. 81.

Krogh, T. E., 1978, Vapour transfer for the dissolution of zircons in a multi-sample capsule, at high pressure, *in* Zartman, R. E., editor, 4th International conference of Geochronology, Cosmochronology, Isotope Geology, 1978: United States Geological Survey, Open-File Report, v. 78–701, p. 233–234.

Krohe, A., 1998, Extending a thickened crustal bulge: toward a new geodynamic evolution model of the paleozoic NW Bohemian Massif, German Continental Deep Drilling site (SE Germany): Earth-Science Reviews, v. 44, p. 95–145.

Kröner, A., and Hegner, E., 1998, Geochemistry, single zircon ages and Sm-Nd systematics of granitoid rocks from the Góry Sowie (Owl Mts.), Polish West Sudetes: evidence for early Palaeozoic arc-related plutonism: London, United Kingdom, Journal of the Geological Society, v. 155, p. 711–724.

Kröner, A., and Willner, A., 1998, Time of formation and peak of Variscan HP-HT metamorphism of quartz-feldspar rocks in the central Erzgebirge, Saxony, Germany: Contributions to Mineralogy and Petrology, v. 132, p. 1–20.

Kröner, A., Wendt, J. I., Liew, T. C., Compston, W., Todt, W., Fiala, J., Vaňková, V., and Vaněk, J., 1988, U-Pb zircon and Sm-Nd model ages of high-grade Moldanubian metasediments, Bohemian Massif, Czechoslovakia: Contributions to Mineralogy and Petrology, v. 99, p. 257–266.

Kröner, A., Byerly, C. R., and Lowe, D. R., 1991, Chronology of early Archean granitegreenstone evolution in the Barberton Mountain Land, South Africa, based on precise dating by single zircon evaporation: Earth and Planetary Science Letters, v. 103, p. 41–54.

Kröner, A., O'Brien, P. J., Nemchin, A. A., and Pidgeon, R. T., 2000a, Zircon ages for high-pressure granulites from South Bohemia, Czech Republic, and their connection to Carboniferous high temperature processes: Contributions to Mineralogy and Petrology, v. 138, p. 127–142.

Kröner, A., Štípská, P., Schulmann, K., and Jaeckel, P., 2000b. Chronological constraints on the pre-Variscan evolution of the northeastern margin of the Bohemian Massif, Czech Republic, *in* Franke, W., Haak, W., Oncken, O., and Tanner, D., editors, Orogenic processes: Quantification and modelling in the Variscan belt: Geological Society of London Special Publication, no. 179, p. 175–198.

Kröner, A., Jaeckel, P., Hegner, E., and Opletal, M., 2001, Single zircon ages and whole rock Nd isotopic systematics of early Palaeozoic granitoid gneisses from the Czech and Polish Sudetes (Jizerske hory, Krkonose Mountains and Orlice-Sneznik Complex): International Journal of Earth Sciences, v. 90, p. 304–324.

Liew, T. C., and Hofmann, A. W., 1988, Precambrian crustal components, plutonic associations, plate environment of the Hercynian fold belt of central Europe: indications from a Nd and Sr isotopic study: Contributions to Mineralogy and Petrology, v. 98, p. 129–138.

Loosveld, R. J. H., and Etheridge, M. A., 1990, A model for low-pressure facies metamorphism during crustal thickening: Journal of Metamorphic Geology, v. 8, p. 257–267.

Ludwig, K. R., 1999, ISOPLOT/Ex version 2.01. a Geochronological toolkit for Microsoft Excel: Berkeley Special Publications Center, Special Publications, 1a.

Macintyre, R. M., Bowes, D. R., Hamidullah, S., and Onscott, T. C., 1992, K-Ar and Ar-Ar study of amphibolites from meta-ophiolite complexes, eastern Bohemian Massif, *in* Kukal, Z., editor, Proceedings of the 1st International Conference on the Bohemian Massif: Prague, Czech Geological Survey, p. 195–199.

Matte, Ph., Maluski, H., Raijlich, P., and Franke, W., 1990, Terrane boundaries in the Bohemian Massif: Result of large-scale Variscan shearing: Tectonophysics, v. 177, p. 151–170.

Matura, A., 1984, Das Kristallin am Südostrand der Böhmischen Masse zwischen Ybbs/Donau und St. Pölten: Jahrbuch der Geologischen Bundesanstalt, v. 127, p. 13–27.

Medaris, L. G., 1999, Garnet peridotites in Eurasian high-pressure and ultrahigh-pressure terranes: A diversity of origins and thermal histories: International Geology Review, v. 41, 799 – 815.

Medaris, L. G., Jelínek, E., and Mísař, Z., 1995a, Czech eclogites: Terrane settings and implications for Variscan tectonic evolution of the Bohemian massif: European Journal of Mineralogy, v. 7, p. 7–28.

Medaris, L. G., Beard, B. L., Johnson, C. M., Valley, J. W., Spicuzza, M. J., Jelínek, E., and Mísař, Z., 1995b, Garnet pyroxenite and eclogite in the Bohemian Massif: geochemical evidence for Variscan recycling of subducted lithosphere: Geologische Rundschau, v. 84, p. 489–505.

Medaris, L. G., Fournelle, J. H., Ghent, E.D., Jelínek, E., and Mísař, Z., 1998, Prograde eclogite in the Gfşhl nappe, Czech Republic: new evidence on Variscan high-pressure metamorphism: Journal of Metamorphic Geology, v. 16, p. 563–576.

Melka, R., Schulmann, K., Schulmannová, B., Hrouda, F., Lobkowicz, M., and Figar, S., 1992, Perpendicular linear fabrics in synkinematically emplaced tourmaline granite: Journal of Structural Geology, v. 14, p. 605–620.

Mezger, K., and Krogstad, E. J., 1997, Interpretation of discordant U-Pb zircon ages: an evaluation: Journal of Metamorphic Geology, v. 15, p. 127–140.

Möller, A., O'Brien, P. J., Kennedy, A., and Kröner, A., 2002, Polyphase zircon in ultrahigh-temperature granulites (Rogaland, SW Norway): constraints for Pb diffusion: Journal of Metamorphic Geology, v. 20, p. 727–740.

Němec, D., 1968, Die Metamorphose des NE-Randes des Kernes der Bşhmischen Masse: Verhandlungen der geologischen Bundesanstalt, v. 1–2, p. 189–203.

O'Brien, P. J., 1997, Garnet zoning and reaction textures in overprinted eclogites, Bohemian Massif, European Variscides: A record of their thermal history during exhumation: Lithos, v. 41, p. 119–133.

O'Brien, P. J., and Vrána, S., 1997, Eclogites with a short-lived granulite facies overprint in the Moldanubian zone, Czech Republic: petrology, geochemistry and diffusion modelling of garnet zoning: Geologische Rundschau, v. 84, p. 473–488.
Oncken, O., von Winterfeld, C., and Dittmar, U., 1999, Accretion of a passive rifted margin: the Late Paleozoic Rhenohercynian fold and thrust belt (Middle European Variscides): Tectonics, v. 18, p. 75–91.
Parrish, R. R., 1987, An improved microcapsule for zircon dissolution in U-Pb geochronology: Isotope Geosciences, v. 66, p. 99–102.
Patočka, F., and Valenta, J., 1990, Geochemistry of metatrachytes and metarhyolites of the southern part of the Devonian Vrbno Group in the Horní Město area and tectonic setting of origin of the metavolcanic protoliths: Časopis pro mineralogii a geologii, v. 35, p. 41–46.
Petrakakis, K., 1997, Evolution of Moldanubian rocks in Austria: Review and synthesis: Journal of Metamorphic Geology, v. 15 (2), p. 203–222.
Pitra, P., and Guiraud, M., 1996, Probable anticlockwise P-T evolution in extending crust: Hlinsko region, Bohemian Massif: Journal of Metamorphic Geology, v. 14, p. 49–60.
Pitra, P., Burg, J. P., Schulmann, K., and Ledru, P., 1994, Late-orogenic extension in the Bohemian Massif: Petrostructural evidence in the Hlinsko region: Geodinamica Acta, v. 6, p. 15–31.
Scharbert, S., and Batík, P., 1985, The age of the Thaya (Dyje) pluton: Verhandlungen der Geologischen Bundesanstallt, v. 3, p. 325–331.
Schulmann, K., 1990, Fabric and kinematic study of the Bíteš orthogneiss (southwestern Moravia) – result of large-scale northeastward shearing parallel to the Moldanubian boundary: Tectonophysics, v. 177, p. 229–244.
Schulmann, K., Ledru, P., Autran, A., Melka, R., Lardeaux, J. M., Urban, M., and Lobkowicz, M., 1991, Evolution of nappes in the eastern margin of the Bohemian massif: a kinematic interpretation: Geologische Rundschau, v. 80, p. 73–92.
Schulmann, K., Melka, R., Lobkowicz, M., Ledru, P., Lardeaux, J. M., and Autran, A., 1994, Contrasting styles of deformation during progressive nappe stacking at the southeastern margin of the Bohemian Massif (Thaya dome): Journal of Structural Geology, v. 16, p. 355–370.
Schulmann, K., Štoudová, S., Konopásek. J., and Martelat, J. E., 1999, Excursion to the Czech part of Moldanubia – The northern margin of the core of the Bohemian massif (processes at boundary of the orogenic root): Beiheft zur European Journal of Mineralogy, v. 11, p. 95–104.
Schulmann, K., Schaltegger, U., Ježek, J., Thompson, A. B., and Edel, J. B., 2002, Rapid burial and exhumation during orogeny: Thickening and synconvergent exhumation of thermally weakened and thinned crust (Variscan orogen in Western Europe): American Journal of Science, v. 302, p. 856–879.
Špaček, P., Kalvoda, J., Franců, E., and Melichar, R., 2001, Variation of deformation mechanisms within the progressive-retrogressive mylonitization cycle of limestones: Brunovistulian sedimentary cover (the Variscan orogeny of the Southeastern Bohemian Massif): Geologica Carpathica, v. 52, p. 263–275.
Steiger, E. H., and Jäger, E., 1977, Subcommission on geochronology, convention of the use of decay constants in geo- and cosmochronology: Earth and Planetary Science Letters, v. 19, p. 321–329.
Steltenpohl, M. G., Cymerman, Z., Krogh, E. J., and Kunk, M. J., 1993, Exhumation of eclogitized continental basement during Variscan lithospheric delamination and gravitational collapse, Sudetes Mountains, Poland: Geology, v. 21, p. 1111–1114.
Štípská, P., and Powell, R., 2005a, Do ternary feldspars constrain the metamorphic conditions of high-grade meta-igneous rocks? Evidence from orthopyroxene gneisses, Bohemian Massif: Journal of Metamorphic Geology.
——— 2005b, Constraining the P-T path of crustal eclogites (an example from the Bohemian Massif): Journal of Metamorphic Geology.
Štípská P., Schulmann , K., and Höck, V., 2000, Complex metamorphic zonation of the Thaya dome: result of buckling and gravitational collapse of imbricated nappe sequence, *in* Cosgrowe, J. W., and Ameen, M. S., editors, Forced folds and fractures: Geological Society of London Special Publication, v. 169, p. 197–211.
Štípská, P., Schulmann, K., Kröner, A., Ježek, J., and Thompson, A. B., 2001, Thermo-mechanical role of Cambro-Ordovician paleorift during Variscan collision. NE margin of the Bohemian Massif: Tectonophysics, v. 332, p. 211–239.
Štípská, P., Schulmann, K., and Kröner, A., 2004, Vertical extrusion and middle crustal spreading of omphacite granulite: a model of syn-convergent exhumation (Bohemian Massif, Czech Republic): Journal of Metamorphic Geology, v. 22, p. 179–198.
Suess, F. E., 1912, Die moravischen Fenster und ihre Beziehung zum Grundgebirge des Hohen Gesenke: Denkschrichte des Koeniglischen Akademie der Wissenscahft, Mathematik, Naturwissenschaft, v. 83, p. 541–631.
——— 1926, Intrusionstektonik und Wandertektonik im variszichen Grundgebirge: Berlin, Borntträger, 269 p.
Svojtka, M., Košler, J., and Venera, Z., 2002, Dating granulite-facies structures and the exhumation of lower crust in the Moldanubian Zone of the Bohemian Massif: International Journal of Earth Sciences, v. 91, p. 373–385.
Synek, J., and Oliveriová, D., 1993, Terrane character of the northeast margin of the Moldanubian zone – the Kutná hora crystalline complex, Bohemian Massif: Geologische Rundschau, v. 82, p. 566–582.
Tait, J., Bachtadse, V., and Soffel, H., 1996, Eastern Variscan fold belt: paleomagnetic evidence for oroclinal bending: Geology, v. 24, p. 871–874.
Tajčmanová L., Konopásek J., and Schulmann, K., 2005, Thermal evolution of the lower crust during exhumation within thickened orogenic root (Variscan belt of Central Europe): Journal of Metamorphic Geology.

Thiele, O., 1976, Ein westvergenter kaledonischer Deckenbau im niederösterechischen Waldviertel: Jahrbuch der Geologischen Bundesanstalt, v. 119, p. 75–81.
Thompson, A. B., 1999, Some time-space relationships for crustal melting and granitic intrusion at various depths, *in* Castro, A., Fernadez, C., and Vigneresse, J. L., editors, Understanding granites: Integrating new and classical techniques: Geological Society of London Special Publication, v. 168, p. 7–25.
——— 2000, Clockwise P/T paths for crustal melting and H_2O recycling in granite source regions and migmatite terrains: Lithos, v. 56, p. 33–45.
Thompson, A. B., Schulmann, K., Ježek, J., and Tolar, V., 2001, Thermally softened continental extensional zones (arcs and rifts) as precursors to thickened orogenic belts: Tectonophysics, v. 332, p. 115–141.
Tollman, A., 1982, Grossräumiger variszischer Deckenbau im Moldanubikum und neue Gedanken zum Variszikum Europas: Geotektonische Forschungen, v. 64, p. 1–91.
van Breemen, O., Aftalion, M., Bowes, D. R., Dudek, A., Mísař, Z., Povondra, P., and Vrána, S., 1982, Geochronological studies of the Bohemian Massif, Czechoslovakia, and their significance in the evolution of central Europe: Transactions of the Royal Society of Edinburgh, Earth Science Series, v. 73, p. 89–108.
Vanderhaeghe, O., Medvedev, S., Fullsack, P., Beaumont, C., and Jamieson, R. A., 2003, Evolution of orogenic wedges and continental plateaux: insights from crustal thermal-mechanical models overlying subducting mantle lithosphere: Geophysical Journal International, v. 153, p. 27–51.
Venera, Z., Schulmann, K., and Kröner, A., 2000, Intrusion within a transtensional tectonic domain: the istá granodiorite (Bohemian Massif)—structure and rheological modelling: Journal of Structural Geology, v. 22, p. 1437–1454.
Vrána, S., 1995, The Moldanubian Zone in the Czech Republic, *in* Dallmeyer, R. D., Franke, W., and Weber, K., editors, Pre-Permian Geology of Central and Eastern Europe: Berlin, Springer, p. 456–460.
Vrána, S., and Kröner, A., 1995, Pb-Pb zircon ages for tourmaline alkali-feldspar orthogneiss from Hluboká nad Vltavou in southern Bohemia: Journal of the Czech Geological Society, v. 40, p. 127–131.
Vrána, S., and Novák, M., 2000, Petrology and geochemistry of granulite clasts in the Visean Luleč conglomerate, Kulm in central Moravia, Czech Republic: Věstník Českého geologického ústavu, v. 75, p. 405–413.
Wendt, J. I., and Todt, W., 1991, A vapour digestion method for dating single zircons by direct measurement of U and Pb without chemical separation: Terra Abstracts, v. 3/1, p. 507–508.
Wendt, J., Kröner, A., Fiala, J., and Todt, W., 1993, Evidence from zircon dating for existence of approximately 2.1 Ga old crystalline basement in Southern Bohemia, Czech Republic: Geologische Rundschau, v. 82, p. 42–50.
Wendt, J. I., Kröner, A., Fiala, J., and Todt, W., 1994, U-Pb zircon and Sm-Nd dating of Moldanubian high-P/high-T granulites from south Bohemia, Czechoslovakia: London, Journal of the Geological Society, v. 151, p. 83–90.
Willet, S. D., Beamont, C., and Fullsack, P., 1993, Mechanical model for the tectonics of doubly vergent compressional orogens: Geology, v. 21, p. 371 – 374.
Williams, I. S., Compston, W., Black, L. P., Ireland, T. R., and Foster, J. J., 1984, Unsupported radiogenic Pb in zircon: a cause of anomalously high Pb-Pb, U-Pb and Th-Pb ages: Contributions to Mineralogy and Petrology, v. 88, p. 322–327.
Winchester, J. A., and The PACE TMR Network Team (contract ERBFMRXCT 97-0136), 2002, Palaeozoic amalgamation of Central Europe: new results from recent geological and geophysical investigations: Tectonophysics, v. 360, p. 5 – 21.
York, D., 1969, Least squared fitting of a straight line with correlated errors: Earth and Planetary Science Letters, v. 5, p. 320–324.
Žák, J., Holub, V. F., and Verner, K., 2005, Tectonic evolution of a continental magmatic arc from transpression in the upper crust to exhumation of mid-crustal orogenic root recorded by episodically emplaced plutons: the Central Bohemian Plutonic Complex (Bohemian Massif): International Journal of Earth Sciences, v. 94, p. 385–400.
Ziegler, P. A., 1986, Geodynamic model for the Palaeozoic crustal consolidation of Western and Central Europe: Tectonophysics, v. 126, p. 303–328.